

REPORT DOCUMENTATION PAGE

Form Approved OMB No. 0704-0188

Public reporting burden for this collection of information is estimated to average 1 hour per response, including the time for reviewing instructions, searching existing data sources, gathering and maintaining the data needed, and completing and reviewing the collection of information. Send comments regarding this burden estimate or any other aspect of this collection of information, including suggestions for reducing the burden, to Department of Defense, Washington Headquarters Services, Directorate for Information Operations and Reports (0704-0188), 1215 Jefferson Davis Highway, Suite 1204, Arlington, VA 22202-4302. Respondents should be aware that notwithstanding any other provision of law, no person shall be subject to any penalty for failing to comply with a collection of information if it does not display a currently valid OMB control number.

PLEASE DO NOT RETURN YOUR FORM TO THE ABOVE ADDRESS.

1. REPORT DATE (DD-MM-YYYY) 18-03-2009	2. REPORT TYPE Final Report	3. DATES COVERED (From – To) 1 Mar 2007 – 28 Feb 2008
--	---------------------------------------	---

4. TITLE AND SUBTITLE Plasma Control of Separated Flows on Delta Wings at High Angles of Attack	5a. CONTRACT NUMBER ISTC Registration No: 3646
	5b. GRANT NUMBER
	5c. PROGRAM ELEMENT NUMBER

6. AUTHOR(S) Dr. Anatoly Alexandrovich Maslov	5d. PROJECT NUMBER
	5d. TASK NUMBER
	5e. WORK UNIT NUMBER

7. PERFORMING ORGANIZATION NAME(S) AND ADDRESS(ES) Institute of Theoretical and Applied Mechanics Institutskaya st. 4/1 Novosibirsk 630090 Russia	8. PERFORMING ORGANIZATION REPORT NUMBER N/A
--	--

9. SPONSORING/MONITORING AGENCY NAME(S) AND ADDRESS(ES) EOARD Unit 4515 BOX 14 APO AE 09421	10. SPONSOR/MONITOR'S ACRONYM(S)
	11. SPONSOR/MONITOR'S REPORT NUMBER(S) ISTC 06-7002

12. DISTRIBUTION/AVAILABILITY STATEMENT

Approved for public release; distribution is unlimited.

13. SUPPLEMENTARY NOTES

14. ABSTRACT

This report results from a contract tasking Institute of Theoretical and Applied Mechanics as follows: At sufficiently high angles of attack the boundary layer globally separates from the leeward surface of delta wing. The flow field contains two strong vortices generated by the roll up of the shear layer emanating from the separation lines near the wing leading edges. For supercritical angles, the vortices demonstrate a large-scale instability accompanied by strong oscillations and eventual breakdown of the vortical structure. This phenomenon, called vortex breakdown or vortex burst, leads to rapid decrease of the lift to drag ratio. If the vortex burst on one wing side occurs earlier than on the other, then strong yawing and rolling moments are induced due to flow asymmetry. It is well known that the leading-edge vortex flow is extremely sensitive to variations of the surface shape and/or external forcing produced near the separation line. Such forcing can be organized by means of dielectric barrier discharge actuators which may be advantageous compared to other modern control techniques (synthetic jets, MEMS and etc.). Dielectric barrier discharge has simple construction, does not change the aerodynamic shape or influence the wing functionality when it is not in use, allows for smooth variations of forcing frequency and power, and can be used for closed loop feedback control. This kind of activation was successfully used for control of boundary-layer separation near the leading edge of a subsonic airfoil at sufficiently high angles of attack. The problem will be studied experimentally in the ITAM low-speed wind tunnel. The experiments will be performed on a delta wing model of approximately 0.5 m chord for flow speeds 10–30 m/s. The model will simulate flow features of the generic "Stingray" UAV model tested with the synthetic-jet actuators. Tests will be conducted at chord Reynolds numbers up to 1 million, which are typical for UAV applications. The large size of the model will help to resolve fine details of the flow field. The experiments will be carried out using modern measurement and visualization techniques. They will demonstrate robustness of plasma dischargers for delta-wing flow control, provide unique database for verification of theoretical and CFD modeling, allow for scaling of this control technique to real flying vehicles.

15. SUBJECT TERMS
EOARD, Aviation Technology, Aerodynamics

16. SECURITY CLASSIFICATION OF:			17. LIMITATION OF ABSTRACT UL	18. NUMBER OF PAGES 40	19a. NAME OF RESPONSIBLE PERSON SURYA SURAMPUDI
a. REPORT UNCLAS	b. ABSTRACT UNCLAS	c. THIS PAGE UNCLAS			19b. TELEPHONE NUMBER (Include area code) +44 (0)1895 616021

ISTC Project 3646

**Plasma Control of Separated Flows on Delta Wings
at High Angles of Attack**

Annual Project Technical Report

on the work performed from Mar 1, 2007 to Feb 28, 2008

**Khristianovich Institute of Theoretical & Applied Mechanics
Institutskaya str. 4/3, Novosibirsk, 630090, Russia**

Project Manager **Maslov Anatoly
Alexandrovich
Dr., Prof.**



Director **Fomin Vasiliy Mikhailovich
Academician, Prof.**



February 2008

This work is supported financially by EOARD and performed under the agreement with the International Science and Technology Center (ISTC), Moscow.

Title of the Project: Plasma Control of Separated Flows on Delta Wings at High Angles of Attack

Contracting Institute: Khristianovich Institute of Theoretical & Applied Mechanics

Participating Institutes: none

Commencement Date: March 1, 2007

Duration: 12 months (the first phase from 24 months of the project)

Project Manager Maslov Anatoly Alexandrovich

phone number: (383) 330 38 80

fax number: (383) 330 72 68

e-mail address: maslov@itam.nsc.ru

1. Brief description of the work plan: objective, expected results, technical approach

The project is relevant to plasma flow control applications, namely, control of flow separation on leading edges of delta (triangular) wings at high angles of attack using barrier plasma discharges. This problem is of critical importance for landing and takeoff of commercial (civil) aircraft. Separation processes on delta wings are relevant to complicated swept wings on such aircraft since the vortex dynamics of the feeding sheets and flow physics is qualitatively similar to that of the basic delta wing flow. The experiments will demonstrate robustness of plasma dischargers for delta-wing flow control, provide unique database for verification of theoretical and numerical modeling.

The project is relevant to fundamental investigations.

The main objectives of this project are:

- Investigate experimentally the efficiency of dielectric barrier discharge actuators for control of pitch and roll of a triangular wing under high angles of attack;
- Investigate vortex structures features and their receptivity to steady and unsteady DBD forcing;
- Estimate the application range of the control technique.

Following results will be obtained at the fulfillment of the project:

- Experimental data on the problem of simulation of delta wing aerodynamics at high angle of attack taking into consideration flow separation and hydrodynamic instability of the vortex structures.
- Experimental data of the barrier discharge physics, and its influence on the boundary layer and vortex structure in the region of separation.
- Data on possibility of asymmetric vortex control by active influence on the pre-separated boundary layer with using of above-mentioned discharge along aerodynamic surface.

The main purpose of the project is to study of possibility to achieve of advantages provided by plasma technologies comparing to other technologies. To prove this fact the experiments in subsonic and supersonic wind tunnels are performed. Subsonic tests are executed in low-turbulence subsonic wind tunnel T-324 of ITAM. Flow velocity range of the facility is 3÷50 m/s, test chamber is of square cross section 1×1 m. Turbulence intensity in the wind

tunnel is sufficiently small ($Tu = 0.04\%$) to extrapolate experimental data to real flight conditions. Supersonic tests will be done in wind tunnel Transit-M for Mach number $M=4$.

Subsonic tests are performed with the model of delta wing (chord $c = 0.3$ m) for flow speed $U_\infty = 10\div 50$ m/s, that corresponds to chord Reynolds number range $Re = 0.2\div 1\cdot 10^6$. The principal experimental techniques are measurements of surface pressure, smoke visualization and balance measurements. Moreover hot-wire measurements will be done to obtain frequency characteristics of shedding vortexes to specify the most effective parameters for DBD actuators. Hot-wire data of mean and instantaneous velocity distributions will give imagination of detailed flow structure in the vortexes. These data will be supplemented by oil-flow visualization on the model surface. Using these experimental methods the flow separation on the leading edge is studied in natural conditions and with excitation by means of DBD. Estimation of DBD control efficiency will be made.

In framework of the project pilot experiments in short duration wind tunnel Transit-M using a model of elliptic cone will be done. The goal of these tests is to demonstrate of possibility of application of plasma discharges for vortex flow control in supersonic flow. The main experimental techniques in this case are balance measurements and flow visualization.

The ITAM team is well equipped to design and fabricate the model, design and install the DBD actuators and perform detailed measurements of flow characteristics. Previous experience of the ITAM team in experimental studies of separated flows will help to achieve the project objectives and minimize the risk.

Two-dimensional DBD actuators of various configurations are used in the project. The actuator consists of two electrodes that are separated by a dielectric material. One of the electrodes is typically exposed to the air. The other electrode is fully covered by a dielectric material. A high voltage A.C. potential is supplied to the electrodes. When the A.C. amplitude is large enough, the air ionizes in the region of the largest electric potential. This generally begins at the edge of the electrode that is exposed to the air, and spreads out over the area projected by the covered electrode. Electrodes may be assembled in various orders against the flow direction, depending of the goal of activation.

The equipment that is necessary to produce barrier plasma discharges includes activators of various types and the two-channel, high-voltage generator that can initiate barrier plasma discharges via two or four channels. The latter can be used to feed plasma discharges of frequencies up to 10 kHz. Our preliminary tests showed that it is feasible to achieve discharges with a power up to 300 W.

The experimental program of subsonic tests includes measurements at various supercritical angles of attack with the DBD actuators off and on. Detailed parametric studies will provide data on the DBD actuator performance and clarify physics of the leading edge separation over delta wings.

The project duration is 24 months, and it includes 6 tasks. The first 12 months are spent to fulfill tasks 1,2,3 and, partially, 4 and 6. In the case of funding extension for the second year (months 13-24) tasks 4,5,6 will be completed.

Short description of project tasks:

Task 1

Estimation of experimental parameters, including selection of model geometry. Sketch design of the model.

Task 2

Manufacturing of the model, model support and 6-component balance adopted for experiments with high voltage in wind tunnels T-324 and Tranzit-M. Assembling and preparation of the pressure measurement system. Preparation of the flow visualization system.

Task 3

Assembling of the model and installation of DBD actuators. Bench testing of plasma discharge system.

Task 4

Wind tunnel tests in T-324.

Task 5

Wind tunnel tests in Tranzit-M.

Task 6

Processing and analysis of data obtained and preparation of final report.

2. Technical progress during the first year

Task 1

Review of published experimental data on effect of vortex burst on delta wings for subsonic flow speed has shown that the burst on a wing with sharp leading edge is to be observed if the angle of attack is close to its critical value. This value depends on aspect ratio

of the wing (ratio s/l , Figure 1). This ratio does not depend on Re number and subsonic flow velocity. According to size of test section of wind tunnel T-324 and possible blockage ratio we have chosen size of the model: sweep angle 65 degrees and chord 300 mm.

Sketch of the delta wing with swept angle $\chi = 65^\circ$ and chord $c = 300$ mm, designed for subsonic tests in T-324 is presented in Figure 2. The model is made from dielectric material Plexiglas and has internal cavity, covered by removable cap. The metal holder attached to the model allows to install it on the strain-gage balance as it shown in the figure. The balance with attached model is fixed in α -turning gear to alter the angle of attack in wide range (Figure 3). Various variants of model designs and actuator layouts were compared. The most perspective actuator consists of Al thin film electrodes and dielectric barrier made from PVC film. The thickness of electrodes must be minimized, width is defined basing on actuator shape. Dielectric barrier may be made from several layers of the film to provide necessary thickness. On the model of delta wing electrodes are glued on leeward side or leeward and windward sides near the leading edge.

Selection of the model for supersonic tests is of considerable difficulty. Due to influence of the flow density on the position of plasma regions, design of the model has to be made taking into account realizable location of plasma discharge filaments. At the phase of sketch design some estimation computations were performed to define loads and choose the method of the flow visualization. For example, it was found that the flow on leeward surface of delta-wing (Figure 5) in supersonic flow has minor effect of the wing lift and moment due to insignificant variation of absolute value of pressure. The flow simulation of 3D flow around elliptic cone for test conditions of supersonic experiment in Tranzit-M was performed by means of commercial software Fluent 6.3.26. The model was an elliptic cone of 250 mm length and base axis ratio 2:1. The structured computational grid consisted of 1.2×10^6 cells was used. Simulation was done assuming laminar boundary layer on the model walls for the following free stream conditions: $P_0 = 10$ bar, $T_0 = 400$ K, $M = 4$. Computations have shown that the flow separation on leeward side of the model begins from $\alpha > 5^\circ$ and pair of primary vortexes is formed. If the angle of attack is further increased, secondary vortexes arise due to backflow and transversal pressure gradient (Figure 4).

The final sketch design of the model for wind tunnel tests in Tranzit-M is presented in Figure 6. The model is an elliptic cone of 250 mm length and base axis ratio 2:1, installed on strain-gage balance. The discrete α -turning gear allows to place the model under various angle of attack. The model is made from dielectric material and electrodes are flush mounted near the model nose.

Task 2

Manufacture of the model

In framework of the task the model of delta-wing for subsonic tests was designed and manufactured. The model is made from dielectric material Plexiglas and has internal volume to place pressure lines and balance holder (Figure 7, Figure 8). The lower cap is made from the same material. The pylon for installation of the model in the test section is a α -turning gear of sector type (Figure 9). Adjustment of α can be performed between wind tunnel runs with accuracy of 0.1° . The pylon is placed on the metal floor of test section and base position of the model is examined by quadrant.

Strain-gage balance measurements

Available 5 and 6-component internal strain-gage balances were adapted for the purpose of the project. 6-component strain-gage balance Э210-379 (Figure 10) are used with the model of delta wing for subsonic tests and 5-component strain-gage balance И2225-244 (Figure 11) will be prepared for supersonic experiments. Additionally, ITAM custom-made strain-gage balance was used for subsonic tests. All necessary holders, screw coupling and other elements have been designed and manufactured.

Measurements of strain-gages signals in course of balance tests was performed by means of one of two acquisition systems. Acquisition unit ECKELMANN (Figure 12), consisting of 26 independent channels will be used for recording of fast processes in Tranzit-M. Each channel includes 14 bit 800 kHz ADC, amplifier and hardware filter. Acquisition system is provided with built-in software which allows to configure each channel, start synchronous recording and export recorded data. The unit is a multi-purpose system for recording of fast processes and is not well fitted for strain-gage balance calibration and measurements, due to large amount of measuring operations of the same kind. Calculation of calibration coefficients and loads is performed by another software basing on the exported data and is possible only after an experiment. Such an attempt makes sense for short duration facilities as Tranzit-M if number of wind tunnel runs is limited.

In subsonic wind tunnel experiments it is necessary and possible to control of measured loads in course of experiment. For this purpose the new acquisition system was designed and assembled. This system allows to measure and observe quasi-steady loads by means of strain-gage balance. Measurement of gage signals is performed by means of multi-channel millimeter Agilent HP34970A. This device provides 24 bit A-D conversion and integration of the signal measured. Acceptable accuracy for experimental conditions can be achieved with integration

time 100 ms per channel. Agilent HP34970A is equipped with GPIB and RS232 communication ports, allowing communication with PC, remote configuration and data transfer.

Special software was developed for this system to make measurements by means of 6-component strain-gage balance.. The software was developed using LabView graphical language and may be used for interactive balance calibration and balance measurements in steady and quasi-steady modes. The software significantly simplifies the procedure of balance measurements in subsonic wind tunnels and allows to monitor loads during the experiment. Screen shot of software interface is presented in Figure 13.

Power supply for the strain-gage balance is of great importance to obtain reliable experimental data. Acquisition system ECKELMANN has internal stabilized 5V power supply. ITAM strain-gage balance has to be supplied by 6 independent 3V power lines. To provide low-noise power supply for this balance it was decided to use 12V rechargeable batteries and specially designed 6-channel voltage regulator.

Coordinate system $O^1X^1Y^1Z^1$ affixed to the balance was used for measurements of aerodynamic loads (Figure 14). Origin of coordinates O^1 is fixed on balance's longitudinal axis and adjusted with electric center of the balance. Position of the moment axes of the balance O^1Y^1 и O^1Z^1 are defined during the calibration. The balance measures forces X^1, Y^1, Z^1 and force moments M^1_x, M^1_y, M^1_z . Then these values are converted to flow coordinate system $Ox_aY_aZ_a$. Origin of coordinates of this system is fixed at conventional center of gravity of the model (in this particular case $X_{c.g.} = 0.2$ m from the model nose). Values of aerodynamic forces and moments affecting the model and measured by balance for stated α can be found solving the following combined equations:

$$\Delta U_{Q_j} = \sum_{i=1}^6 K_{Q_j}^{Q_i} Q_i, j = 1 \div 6,$$

where $Q_1 \div Q_6$ are loads in balance coordinate system. Then load coefficients in the balance coordinate system can be found according the following formulae:

$$C_x = \frac{X^1}{qS}, \quad C_y = \frac{Y^1}{qS}, \quad C_z = \frac{Z^1}{qS},$$

$$m_x = \frac{M_x^1}{qSL}, \quad m_y = \frac{M_y^1}{qSL} + \frac{X_{cg} - x_0^1}{L} C_z, \quad m_z = \frac{M_z^1}{qSb_a} - \frac{X_{cg} - x_0^1}{b_a} C_y, \text{ где}$$

$q = \rho U^2 / 2$ -dynamic pressure,

S – model area ($S=0.5*L*b_0=0.42m^2$),

L -wing span, b_0 -root chord,

$b_a = 2/3 * b_0 = 0.2 \text{ m}$ – mean aerodynamic chord,

X_{cg} – coordinate of the model center of gravity (0.2 m from the model nose),

X_0^I – coordinate of electric center of the balance (0.2566 m).

To convert this data to the flow coordinate system the following relations were used:

$$C_{xa} = C_x \cos(\alpha) + C_y \sin(\alpha)$$

$$C_{ya} = C_y \cos(\alpha) - C_x \sin(\alpha)$$

The rest of coefficients are the same for balance and flow coordinate system.

Pressure measurements

Distribution of pressure on the surface of model can give an important information both on details of the flow and on integral aerodynamic characteristics of model. In the framework of the project two different techniques of pressure measurement are used. The classical technique assumes pressure ports in the model surface and measurement of the pressure by strain gauges installed inside of the model or placed outside and connected with pressure ports by means of pneumolines. Restrictions of the given method are well-known and described in the literature. First of all, it is difficulty of maintenance of the necessary spatial resolution and high cost if number of pressure points is significant. Nevertheless, this method possesses high reliability and is used in the project. Gauges TDM-4D have a range 0.01 MPa which completely overlaps the values of pressure during experiments in T-324. For measurement of gauge signals we use scanning 24 bit multimeter Agilent HP34970A operated by a personal computer. For supervision of gauge data during experiment, their calibration and record of experimental data special software was developed. The interface of this software is shown in Figure 15.

Furthermore in experiment another technique based on application of scanning probe was used. The photo of the probe shown in Figure 16. The probe is a needle of diameter 0.8 mm with an aperture turned to a surface of model moved by means of the traversing gear (Figure 17). Thus the probe is pressed to a surface it measures the pressure in surface layer. In the experiment pressure was measured by differential pressure gauge Omega PX2650-10D5V as a difference between Pito pressure in the test chamber and pressure in the probe described above. Preliminary experiments on a model of wing equipped with surface pressure ports (chord 100 mm, speed $U_\infty = 10 \div 22 \text{ m/s}$) have shown that within 15÷100 % of the model chord difference between indications of the probe and surface pressure ports does not exceed 5% of dynamic pressure. This testing was made by means of a column manometer. Basing on hot-wire data obtained in the boundary layer in is possible to conclude that dynamic pressure does not exceed 5 % of q_∞ at the height of the probe. Doubtless advantage of the technique is the

opportunity to obtain of detailed distribution of pressure on the whole surface of the model. Control of movement of the probe and data gathering were carried out by means of computer manually or automatically.

Visualisation techniques

Visualization of the flow near the surface allows to discover such interesting features and flow singularities as separation and attachment lines, nodes and saddle points. Oil-flow visualization is especially fruitful for study of vortex flows. In subsonic tests we used mixture of fluorescent dye and kerosene brushed on the model surface, strokes were oriented across the main flow direction. The model was exposed in the flow until complete evaporation of kerosene and then the model was photographed. To increase of the image contrast the model surface was painted in black color. An example of oil-flow visualization is presented in Figure 18.

More detailed image of vortex development and breakdown on the leeward side of the wing may be obtained by means of laser sheet technique. This technique is based on injection of light-scattering particles into the flow upstream of the model. Regions of high concentration of particles are revealed by means of laser illumination. If the laser beam is expanded in one dimension by means of two-dimensional lens the concentration of particles is visualized in the plane of laser sheet. Sketch of this technique is shown in Figure 19. The smoke is injected far upstream of the model to minimize the possible influence on the flow. Video recording of visualization is performed by means of the camera installed on the pylon downstream of the model. Though the particle concentration is not connected directly to gasdynamic parameters of the flow its analysis is very useful for understanding of flow topology. Primary and secondary vortices can be easily discovered in the images. Moreover locations of the vortex cores and their size can be seen allowing to identify the vortex status. Application of laser sheet scanning the flow along x coordinate allows to define the position of the primary vortex breakdown. This technique is inertialless in contrast to oil-flow visualization and surface pressure measurements so it has doubtless advantages in experiments with electric discharges.

Within this task the smoke injection system was designed to use in subsonic wind tunnel T-324, selection of light sources and cameras to record of visualization image was made. All necessary tests were done to examine efficiency of the system and to define limits of their application.

Task 3

Dielectric barrier actuator is relatively simple device therefore, it is possible to make and test many variants of it. Design of all DBD actuators is the same, only shape, number and position of the electrodes are different. Examples of the actuators installed on leeward side of the model are shown in Figure 23 and Figure 24. Here two variants with electrode along and across the leading edge are presented. The actuators installed on the right and left wings were always connected to different high-voltage generators.

All actuators installed on the model are of the same design which is outlined in Figure 21. The encapsulated electrode is a strip of aluminium foil of thickness $5\ \mu\text{m}$ glued on the model surface. Several layers of $8\ \mu\text{m}$ lusterless PVC are placed over it. The surface structure of the film is very important for successful creation of dielectric barrier discharge. Stable streamers are formed on the dielectric surface if some glossy material is chosen. Location of these streamers is permanent and disruption of dielectric is often happens as a result of local overheating. Application of lusterless dielectric films is favorable to diffusing the discharge and increasing of lifetime of the actuators. Total thickness of the dielectric layer is chosen as a compromise between maximum gradient of electric field and maximum lifetime of the actuator. Generally it is assembled from three layers of the film allowing to use the actuator during the whole series of experiment. Relative positions of the encapsulated and exposed electrodes were varied. An actuator with overlapped electrodes is less effective but more reliable and long-living due to less heat loads. Moreover overlapping of electrodes allows to easily achieve uniformity of discharge along the electrodes. In the most of tests electrodes were overlapped by $1\div 1.5\ \text{mm}$.

In subsonic tests DBD actuators are fed from high-voltage generators developed and made by ITAM. Schematic diagram of this device is shown in Figure 25, Photo is presented in Figure 26. The generator is a monoblok device and was designed to create of electric discharges of barrier type. It consists of carrier generator, system of keys T1-T2 and step-up transformer. Output voltage may be varied in range of $6\div 10\ \text{kV}$, pulse frequency range is $400\div 10000\ \text{Hz}$. There is possibility to use external carrier frequency generator and to control of internal generator by external signal. Using these options it is possible to implement burst mode of high voltage generation. In this case, bursts of pulses of carrier frequency f are generated with frequency F and defined duration. Examples of voltage oscillograms for continuous generation and burst mode are presented in Figure 27 — Figure 29. It is necessary to mention that key system imposes a limitation on the carrier frequency. Since the combination of transformer and actuator is an oscillatory circuit, excitation of discharge with low frequency produces additional oscillation with self frequency of the system. (Figure 27). If

the frequency is increased the resonance can be achieved and the generator operates in harmonic mode. (Figure 28). The DBD actuator is a capacitor of variable value so self-frequency of the system is defined by configuration of the actuator and other parameters such as area of electrodes, overlapping, thickness and material of the dielectric layer. It depends also on plasma parameters because plasma represents an additional electrode, and consequently it depends on voltage, pressure, frequency and etc.

Successful wind tunnel tests are possible only if electronic compatibility of the measurement and high-voltage equipment involved is provided. The recent experiments discovered that DBD usually does not create significant electronic noise for measurement equipment. An example of strain-gage balance signal for active DBD is presented in Figure 30. It is possible to see that the discharge produces harmonic noise with frequency of discharge (1 кГц). This noise can be easily filtered by bandwidth filter or eliminated by averaging of the signal. At the same time all high voltage connections have to be made carefully as they strongly affect the noise level.

Elimination of electric noise in supersonic tests is more difficult. First of all discharge power in such test is much higher and estimated as several hundred watt. Since the run time of Tranzit-M is about 100 ms, using of signal averaging is not possible. If planned to use an impulse power source for discharge therefore signal filtering is also difficult.

All necessary efforts were performed for breadboard design of high-voltage cables disposition inside models and pylons. Figure 31 demonstrates bench testing setup for examination of compatibility of the strain-gage balance and data acquisition system with high voltage discharge initiated in Mach 2 flow. Tests were done for static pressure equal to one in test chamber of Tranzit-M. It was found that the level of electric noise is significant and additional efforts are needed to obtain reliable experimental data.

Task 4

In framework of the task during the first year of the project subsonic wind tunnel experiments were performed. Figure 32 demonstrates photo of the experimental model installed in the test section of T-324. The model is fixed on the pylon under positive angle of attack. Video camera used for laser sheet visualization is attached to the same pylon. The smoke injection tube is placed upstream of the model by means of magnet holder. The Pitot tube is located upstream of the model near the floor of the test section.

Figure 37 shows the prints of oil-flow visualization. From the photos it is possible to see the separation lines of secondary S_2 and tertiary S_3 vortices. The separation line of the primary vortices is supposed to be on the leading edge of the delta wing. The attachment lines are less distinctive. Their location can be found basing on the analysis of the streamlines visible in the photos. For example, for the angle of attack 15° (Figure 33a) stream lines near the model centerline are straight and directed from the model apex to the trailing edge. Going away from the centerline it is possible to see that at some angle streamlines begin to curve. Combined analysis of oil-flow data with laser sheet visualization data allows to conclude that for moderate angles of attack there are two separate attachment lines of the primary vortices A_1 . Therefore there is the region of the flow not involved in rotational motion between the vortices. This region was found at least up to $\alpha = 21^\circ$, there winding of the streamlines can be found directly near the centerline. It is possible to conclude that attachment lines A_1 of the right and the left primary vortices are merged with increasing of α .

It is possible to see from Figure 33 that the flow on the leeward surface of the model is not conical in the whole range of the angle of attack. Lines of secondary separation S_2 are curved to the centerline for $\alpha = 15 \div 20^\circ$. Evident bent of S_2 may be found at $\alpha = 20^\circ$ and bent point moves to the model apex as the angle of attack increased. Such bent usually connected with the point of breakdown of the primary vortex. More detailed investigation of the photos of Figure 33, allows to discover presence of tertiary vortices along the model leading edge.

It was shown above that in the leeward side of the model there is a flow with domination of two primary vortices. Flow visualization by means of laser sheet allows to discover position of vortex cores and the state of them. Comparison of oil-flow and laser sheet visualization data allows to imagine a conception of the flow pattern. The plane of the laser sheet is oriented transversely to the model surface and the sheet was moved in streamwise direction from the model nose to the trailing edge to obtain more information in the same experiment. Figure 34 - Figure 36 show combined flow visualization data obtained by means of oil-flow and laser sheet techniques. Three typical flow patterns obtained for $\alpha = 15, 17$ and 22° are shown. The primary vortices can be discovered in all images, their cores are seen as dark regions in the center of the vortices.

If the angle of attack is moderate ($\alpha = 15^\circ$) the vortex cores are seen up to the trailing edge where they are destroyed due to positive pressure gradient. The breakdown of the right vortex is usually happens a little close to the model apex. Such a tendency was found in all tests and may be produced by systematic error of the model installation or slight asymmetry of the model. The separation line of the secondary vortex does not have sharp bend and smoothly

curved to the centerline. In sections of the laser sheets presented in Figure 34 and Figure 35 the secondary vortexes can be discovered as area of high smoke concentration under the primary vortexes. The secondary vortex also presents in section $x/c = 0.95$ of Figure 35, where the core of the primary vortex disappeared. This fact corresponds to oil-flow data which show absence of sharp bent points of S_2 line for $\alpha = 17^\circ$.

If the angle of attack is further increased the primary vortexes undergo breakdown near the trailing edge of the model and position of breakdown moves upstream with increasing of α . Figure 35 shows that for $\alpha = 17^\circ$ the point of vortex breakdown defined as the point of disappearance of dark center of the vortex take place at $x/c = 0.77$. Further increase of α results in earlier vortex breakdown. It is possible to see from Figure 36 that in the section $x/c = 0.9$ the primary vortex is destroyed and secondary vortex can not be found.

Dependence of the primary vortex breakdown location on the angle of attack for flow speed $U_\infty = 14$ m/s is shown in Figure 37. The position of S_2 bent point obtained from oil-flow data for $U_\infty = 12$ m/s is also plotted on the graph. It is possible to see that there is some correlation between of breakdown position and S_2 bent. It is known that vortex breakdown results in sudden deceleration of the flow and expansion of the vortex. Therefore breakdown of the primary vortex leads to displacement of secondary vortex to the leading edge and bent of S_2 line. For the angle of attack less then 21° position of the bent was found downstream form the point of breakdown. This fact is probably connected with unsteady character of the breakdown. Moreover the expansion of the vortex after disappearance of the dark vortex core takes some time and space.

Positions of the vortex cores for $\alpha = 12^\circ, 15^\circ, 17^\circ$ and 20° obtained from laser sheet visualization for $U_\infty = 12$ m/s are presented in Figure 38. Red lines are vortex positions in 3D space and blue lines represent their projection on the model surface. Data are presented for all combinations of sections and the angle of attack where it is possible to determine the dark region of the vortexes. It can be seen from these data that the flow is not conical for $\alpha = 12^\circ$ and 15° . The vortex cores rise over the model surface with increasing of coordinate x and move to the leading edge. This corresponds to oil-flow data showing the curve of S_2 line to the centerline with rising of the primary vortex. The flow is near conical for $\alpha = 17^\circ$, vortex core lines and their projections are more close to strait lines. The same behavior may be found for $\alpha = 20^\circ$ up to vortex breakdown position.

Balance measurements of the model of delta-wing were done in range of $\alpha = 10^\circ \div 40^\circ$ for several values of the flow speed 12, 21.6, 33.2 m/s. These data are presented in Figure 42. Drag coefficient C_{xa} , lift coefficient C_{ya} , side force C_{za} , lift/drag ratio K , pitch moment

coefficient m_{za} and roll moment coefficient m_{xa} are shown here. All data are converted to flow coordinate system.

It is possible to see from the graph $C_{ya}(\alpha)$ that lift force is increasing with increasing of the angle of attack and maximum was achieved at $\alpha = 30^\circ$. The data obtained for different flow speeds are well coincided. Maximum lift coefficient was obtained for $U_\infty = 33.2$ m/s. With decreasing of the flow speed up to 12 m/s it was found that C_{ya} decreases for the whole range of the angle of attack. It is interesting to note the break of curves near $\alpha = 20^\circ$, obtained for all studied flow speeds. This behavior of the lift force is produced by motion of the vortex breakdown point with change of the angle of attack. For moderate α the vortex breakdown take place downstream of the model trailing edge. With increasing of the angle of attack the breakdown point moves upstream and crosses the trailing edge at some α , producing the break on the $C_{ya}(\alpha)$ curve. Complete destruction of vortex structure on the leeward surface of the model and formation of closed separation bubble was obtained at $\alpha = 30^\circ$.

Drag of the model increases with the angle of attack and has maximum at $\alpha = 35^\circ$. The curve $C_{xa}(\alpha)$ for $U_\infty = 12$ m/s is situated higher then other data obtained for higher flow speeds that results in corresponding effect on lift/drag ratio. Values of side force and roll moment are negligible and data spread increases with decreasing of the flow speed due to great effect of experimental errors for low speed.

Is possible to see from the plot of pitch moment coefficient that center of pressure moves to the model nose as the angle of attack increases and this results in increase of m_{za} . There is no evident change of curve behavior when the vortex breakdown cross the trailing edge of the model. The maximum of m_{za} was obtained at $\alpha = 35^\circ$, that corresponds to global separation on the leeward side of the model. In this case, the separation bubble is formed and suction on this side significantly decreases. Windward side begins to play greater role in creation of lift force. This results in shift of the center of pressure downstream and decreasing of m_{za} .

An attempt to simulate the effect of active DBD by means of surface turbulizer was made. The turbulizers were placed as it is shown in Figure 41. Figure 39 and Figure 40 presents distributions of pressure coefficient C_p , measured on the leeward side of the model using the scanning pressure probe described above. The data are presented for two test cases for comparison: clean model and the model with one turbulizer. In the latter case, the turbulizer was a string of 0.7 mm diameter placed perpendicularly to the leading edge at distance 50 mm from the model nose. The length of the turbulizer was the same as distance from the leading edge to the centerline.

Symmetric vortex pattern was obtained for the case of clean model, as can be seen from the Figure 39 where there are two suction peaks from the primary vortices of equal width and strength. Additionally there are less pronounced suction peaks produced by secondary vortices near the leading edge on both halves of the wing. If turbulizer was installed the breakdown provoked by the turbulizer increases the vortex diameter and results in widening of the right suction peak (Figure 40). In this case, the peak produced by the secondary vortex was found only on the left side of the model. Absence of this peak may be explained by displacement of the vortex to the leading edge or complete disappearance of the vortex.

Installation of several turbulizers as shown in Figure 41 results in earlier vortex breakdown. In the case of clean model for $U_\infty = 12$ m/s and $\alpha = 17^\circ$ position of the breakdown is $x/c_{break} = 0.8$. Installation of one turbulizer shifts it upstream to $x/c_{break} = 0.66$, and installation of two results in $x/c_{break} = 0.58$. Installation of the third additional turbulizer does not give an effect.

As a part of the task activity the series of DBD vortex control experiments were performed. The actuators were placed symmetrically on both (right and left) sides of the model and were fed independently by different generators of the same type. During the first year of the project, we made experiments using actuators of various shapes. The main efforts were applied to test three different actuators:

DBD actuator along the leading edge

The encapsulated electrode is placed on the leeward side of the model directly on the leading edge. Width of the electrode is 8 mm, the overlap is 1 mm, so the distance from the exposed electrode to the leading edge is 7 mm. Electrodes begin at 25 mm from the model nose and end at 25 mm to the trailing edge. This limitation is necessary to prevent dielectric breakdown at the edge of dielectric. The actuator assembled in that way produces periodic blowing of the air to the leading edge direction. The photo of the model with actuators of such kind is shown in Figure 23, and example of the smoke visualization is presented in Figure 43. One of options of this type was the actuator with electrodes placed on both windward and leeward model surfaces in such a way to create the flow to the leading edge. In both cases attempts to create the plane pulsing jet directed perpendicularly the leading edge were performed. According to the estimations this jet is able to excite the vortex sheet shedding from the leading edge.

The experiments have shown that this configuration is not effective from the point of view of the vortex flow control on the leeward side of the delta wing. It is possible to see from laser sheet and oil-flow visualization data that in this case the actuator is placed in the region of

separated flow and is not able to make significant influence on the main flow. The additional flow induced by actuator is not sufficient for vortex flow control for the flow speed more than 10 m/s.

DBD actuator near S_2 line

It was intended to place an actuator directly upstream of the separation line of the secondary vortex to excite it and consequently the primary vortex. Since S_2 line is inclined to the model centerline at an angle about 18° , the actuator was placed at angle 14° . Two variants of the actuator were tested: asymmetric with induced flow direction to the centerline (Figure 44) and symmetric, representing a plane synthetic jet shown in Figure 45. In the latter case the distance between exposed electrodes was 8 mm. Width of exposed electrodes was 7 mm, overlap was 1 mm. Electrodes begin at 25 mm from the model nose and end at 50 mm to the trailing edge.

Experiments were done for various regimes of actuation including continuous and burst modes. In the whole test range of $\alpha = 10^\circ \div 35^\circ$ and flow speed $U_\infty = 3 \div 30$ m/s we did not find significant effect on the vortex breakdown or vortex positions.

DBD actuator across the leading edge

The photo of the model with installed actuators of this kind is presented in Figure 24. There are 6 actuators on each side of the model fed separately by two generators. The actuators are distributed on the model surface with distance between them about 30 mm. Actuators are oriented across the leading edge and the exposed electrodes are located downstream. The goal of experiments was to excite the primary vortex to induce earlier breakdown.

The experiments were performed in the range of flow speed $10 \div 30$ m/s, angle of attack was varied from 10° to 25° . It was found that this type of actuator is the most successful for the vortex flow control. Figure 46 demonstrates an example of laser sheet visualization for active actuator on the right side. It is possible to see that the left vortex has evident core and at the same time the right vortex does not have a stable core. The control effect is very similar to one obtained with turbulizers. The effect was achieved for wide range of the flow speed and the angle of attack.

3. Current technical status

- Project is on schedule.

4. Cooperation with foreign collaborators

- trips to/from foreign collaborators

The meeting with Surya Surampudi, representative of EOARD was organized during the 46th AIAA Aerospace Sciences Meeting and Exhibit, January 7-10, 2008

- Workshops, topical meetings organized by the project team

Workshops of the project participants in general were assembled weekly.

5. Perspectives of future developments of the research/technology developed

The study performed in the framework of the project concerned application of plasma for flow control on the delta-wing are of great importance for improvement of cost efficiency and flight safety of commercial airplanes. Processes of the flow separation on the delta-wing is relevant to swept wings of the modern airplanes due to similar vortex dynamics and flow physics to the fundamental case of the delta-wing. The experiments have demonstrated efficiency of plasma discharges for the flow control on the delta-wing and will provide database for verification of theoretical and computational models.

Attachment 1

Illustrations to the main text

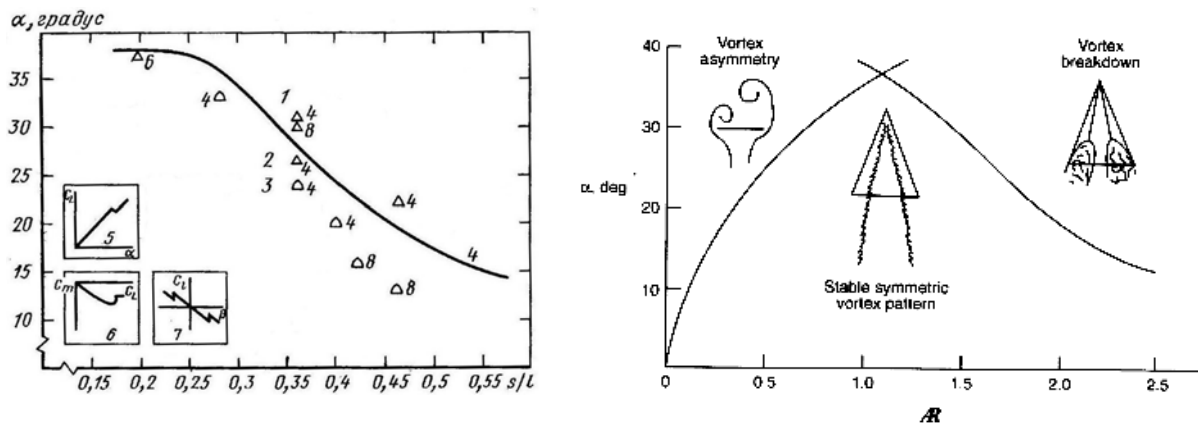


Figure 1 Flow regimes of the delta wing

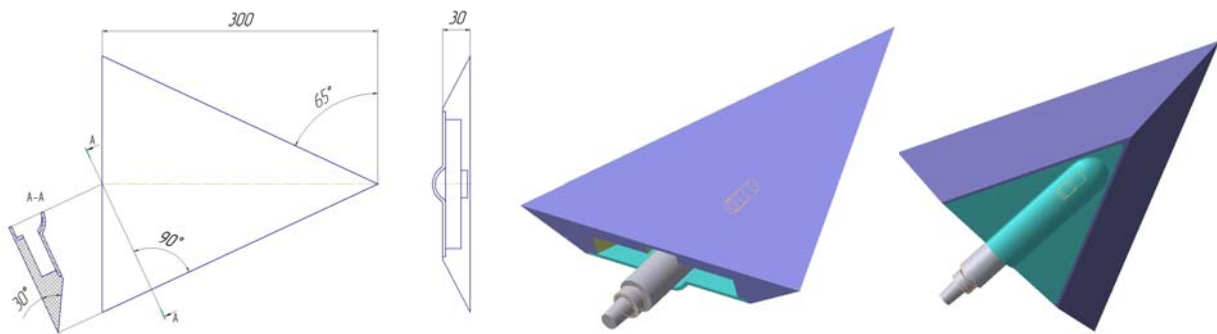


Figure 2 Draft of the delta wing model for tests in wind tunnel T-324

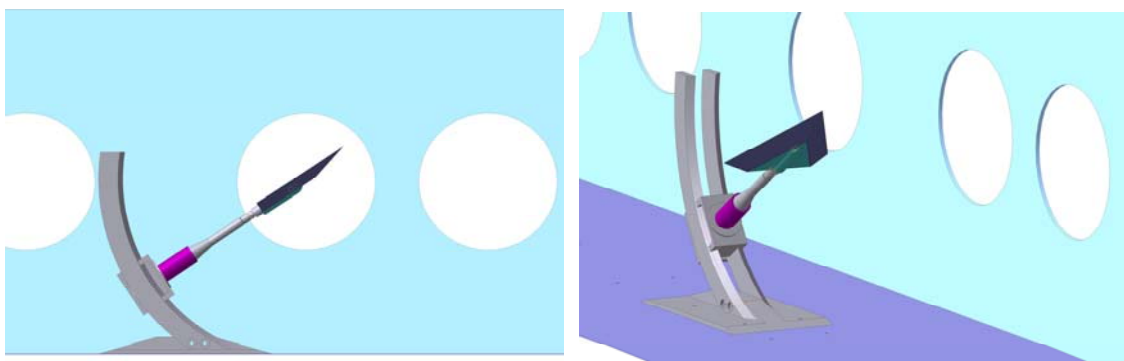


Figure 3 General layout of the model in test section of T-324

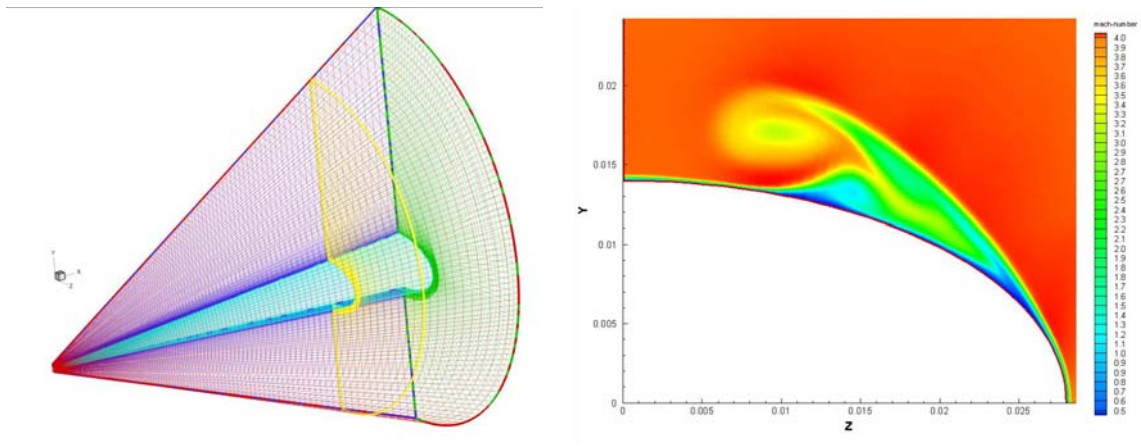


Figure 4 Computation grid and computed Mach number on the leeward side of elliptic cone ($\alpha = 10^\circ, x = 200 \text{ mm}$)

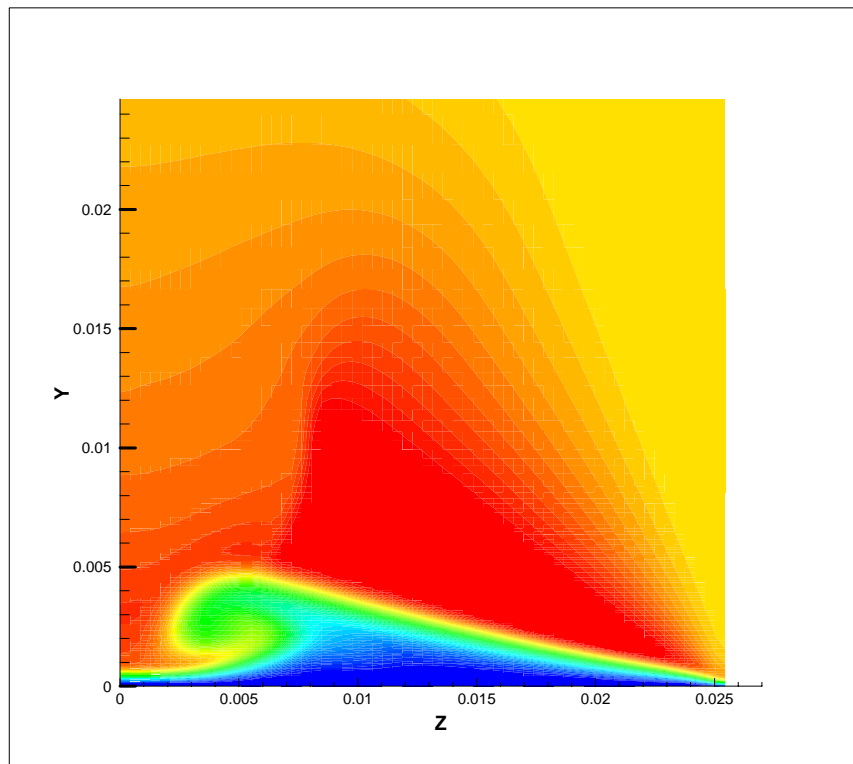


Figure 5 Computed Mach number on the leeward side of the plane delta wing ($M_\infty = 4, \alpha = 15^\circ, x = 70 \text{ mm}$)

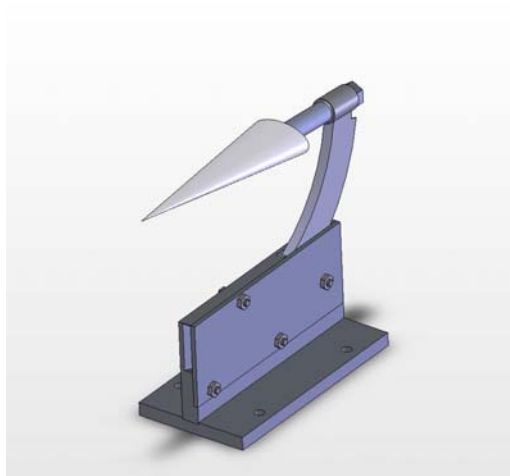


Figure 6 Draft of the elliptic cone model for tests in wind tunnel Tranzit-M

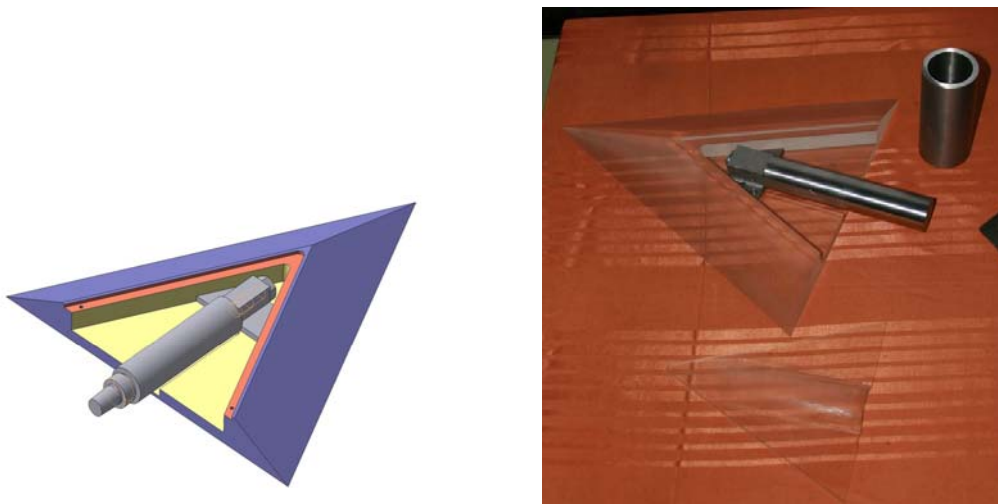


Figure 7 CAD project and photo of the delta-wing before assembling

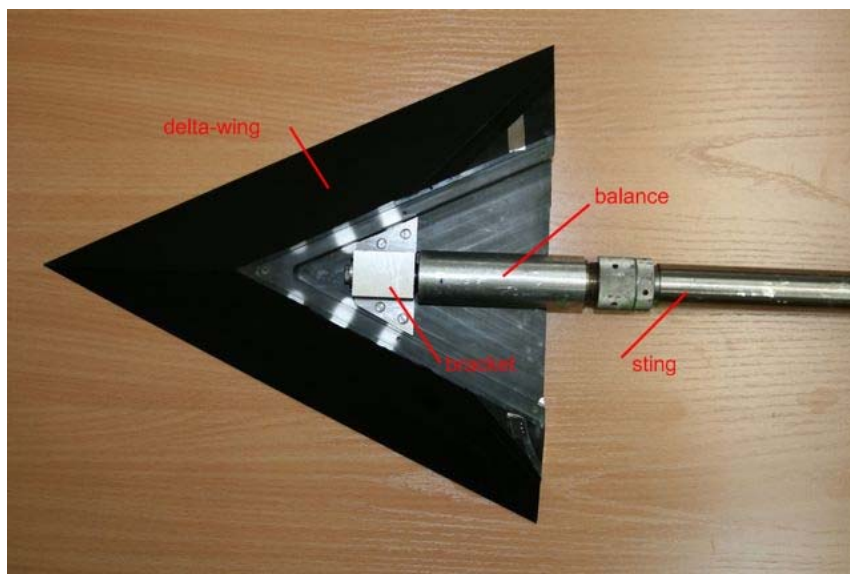


Figure 8 Assembled delta-wing



Figure 9 Photo of the delta-wing installed on the pylon

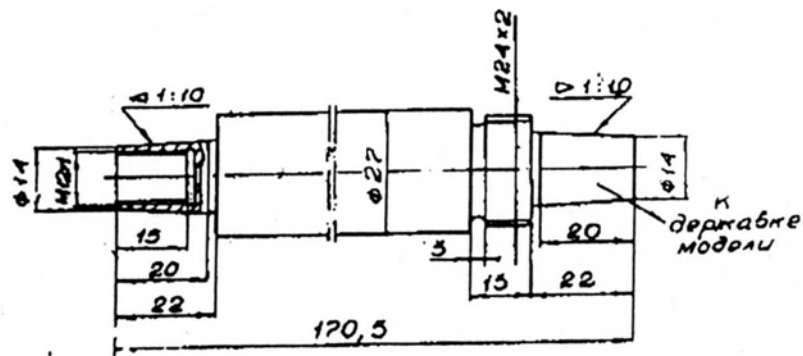


Figure 10 6-component strain-gage balance Э210-379

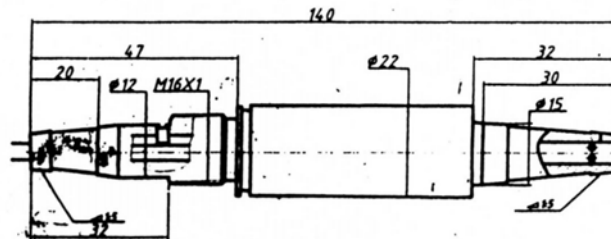


Figure 11 5-component strain-gage balance И2225-244



Figure 12 Acquisition system ECKELMANN

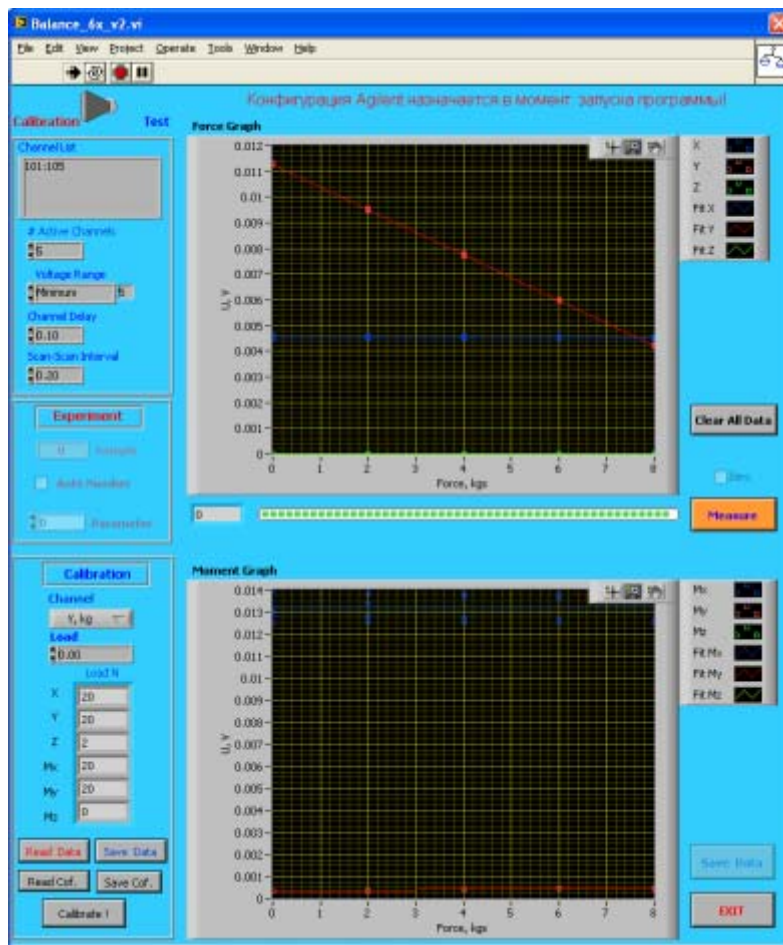


Figure 13 Screen shot of strain-gage measurement software

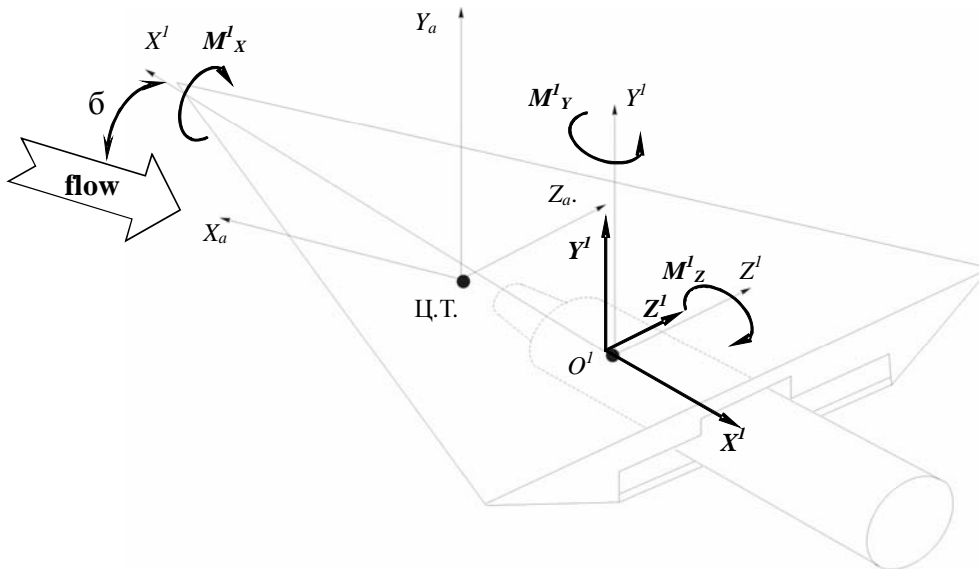


Figure 14 Coordinate system for balance measurements

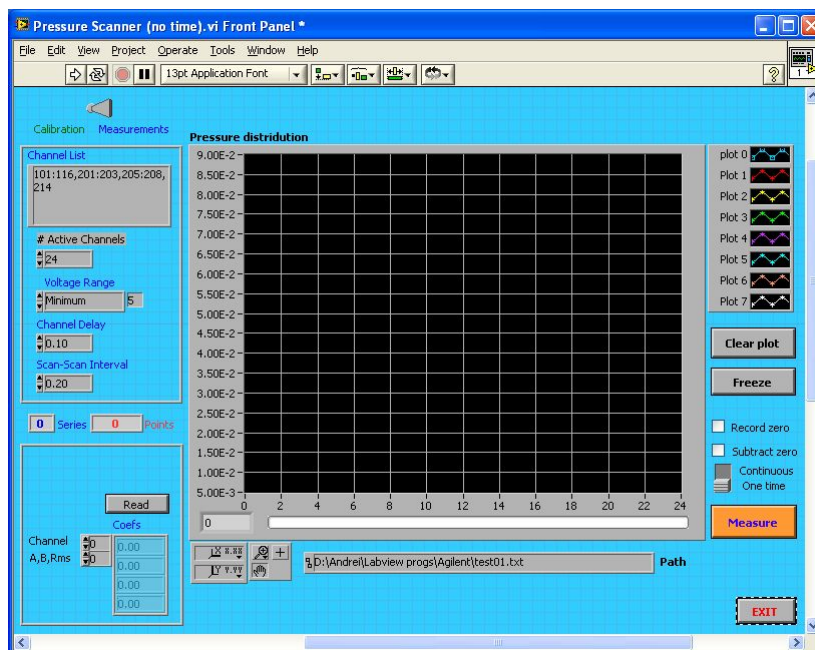


Figure 15 Screen shot of pressure measurement software



Figure 16 Surface pressure probe

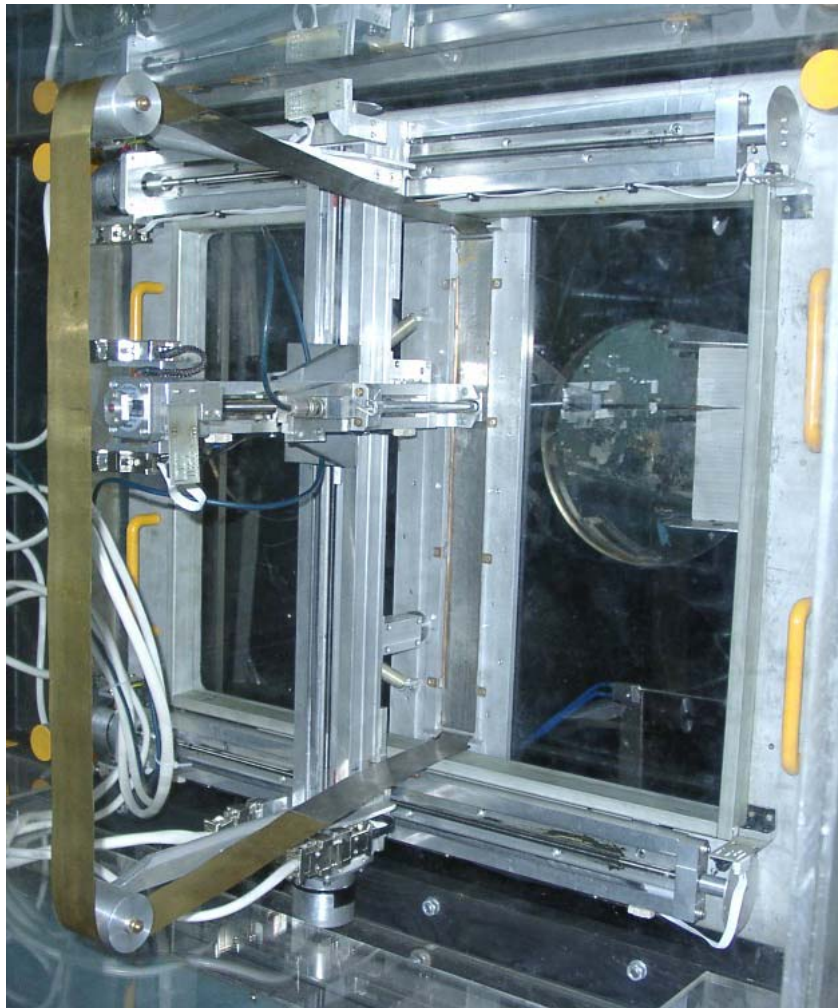


Figure 17 Traversing gear of T-324

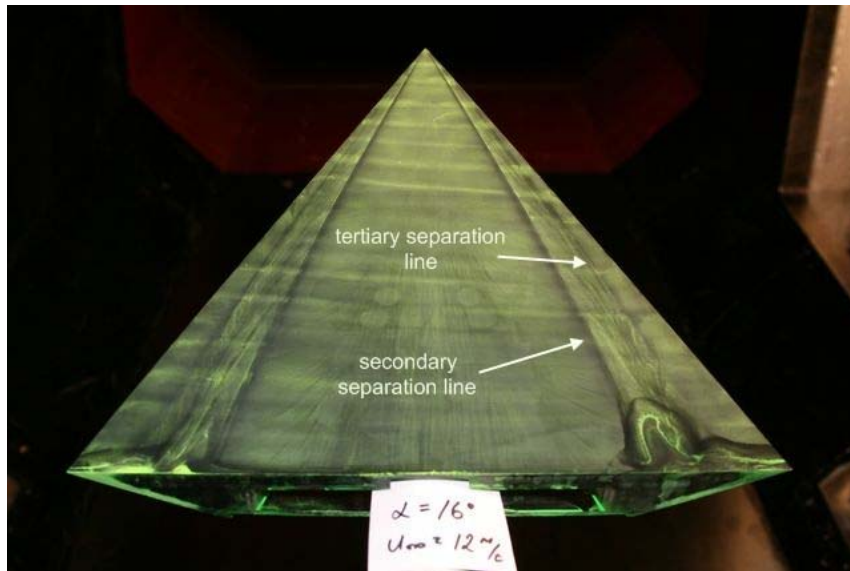


Figure 18 Oil-flow visualization on the delta-wing model

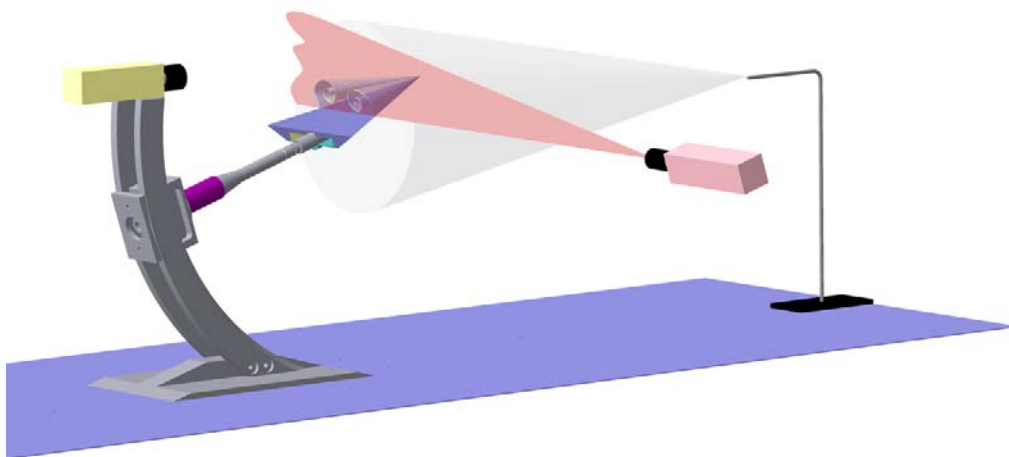


Figure 19 Layout of laser-sheet smoke visualization

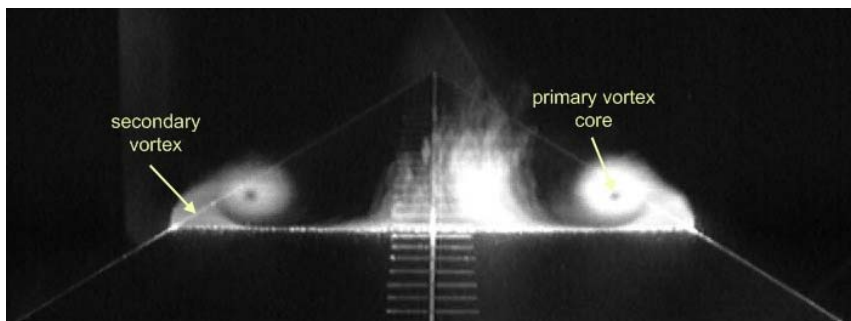


Figure 20 Laser-sheet smoke visualization

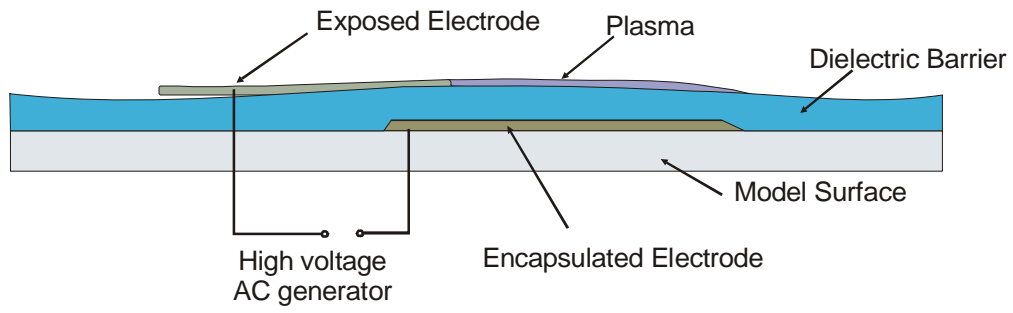


Figure 21 Scheme of dielectric barrier discharge

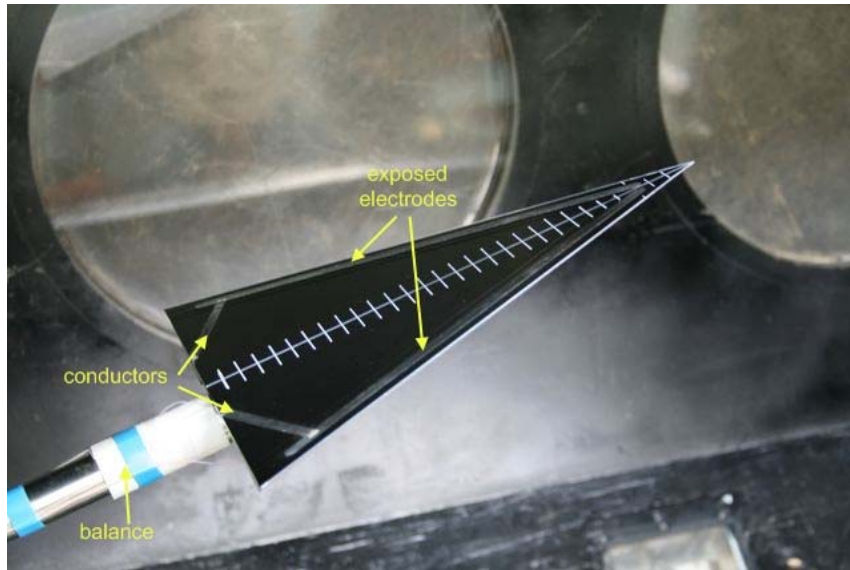


Figure 22 Assembled model

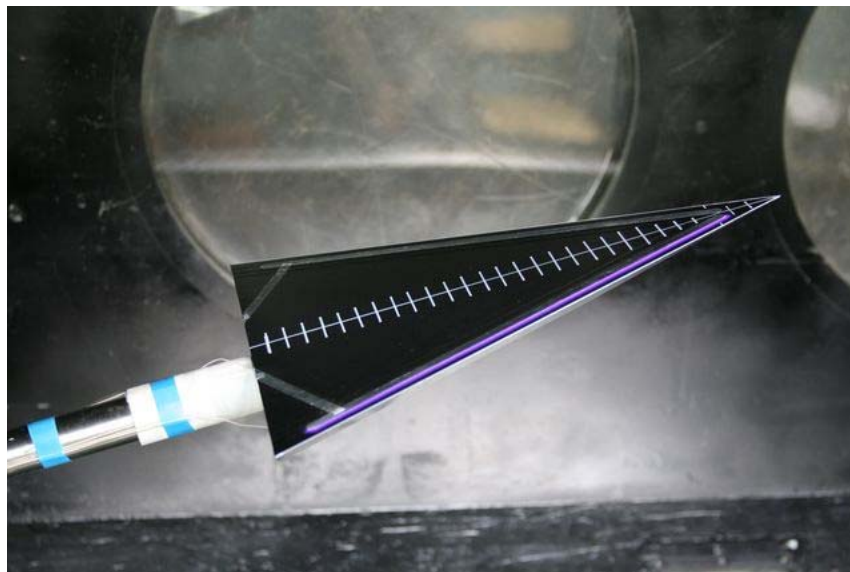


Figure 23 Actuators along the leading edge

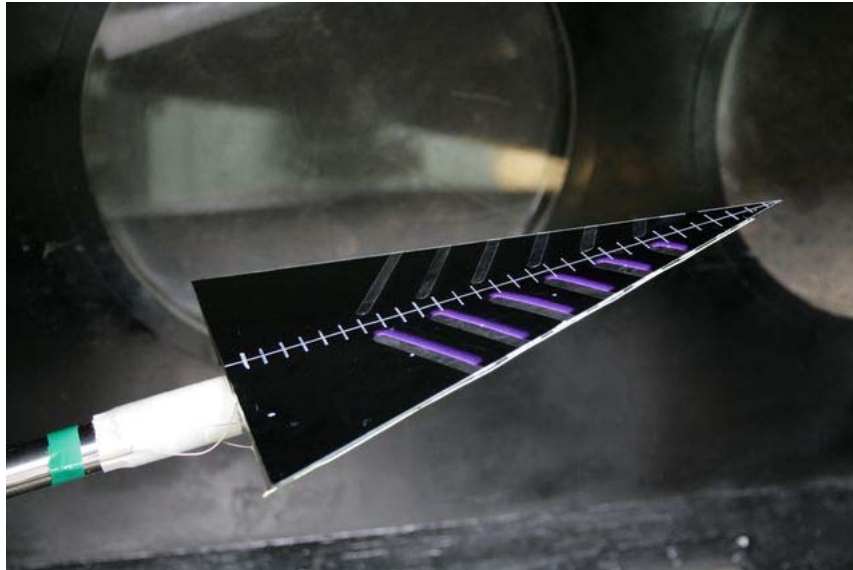


Figure 24 Actuators across the leading edge

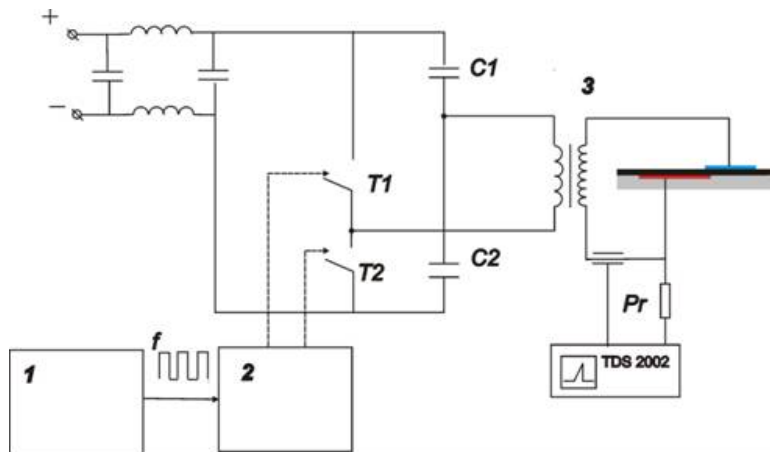


Figure 25 Electric scheme of the high-voltage generator



Figure 26 Photo of the high-voltage generator

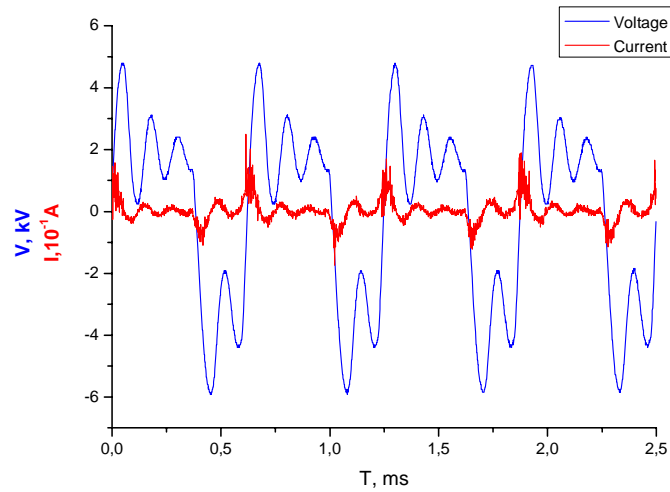


Figure 27 Oscillograms of voltage and current on the actuator ($f = 1600 \Gamma \text{H}$)

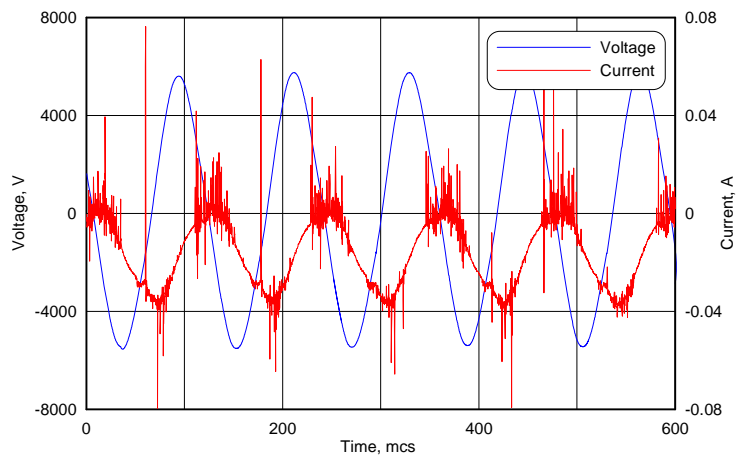


Figure 28 Oscillograms of voltage and current on the actuator ($f = 8333 \Gamma \text{H}$)

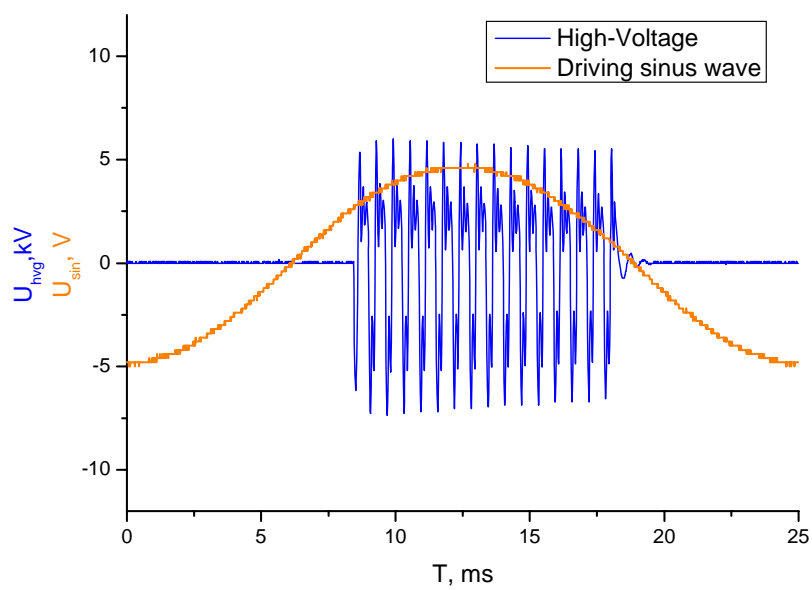


Figure 29 Oscillograms of voltage in burst mode

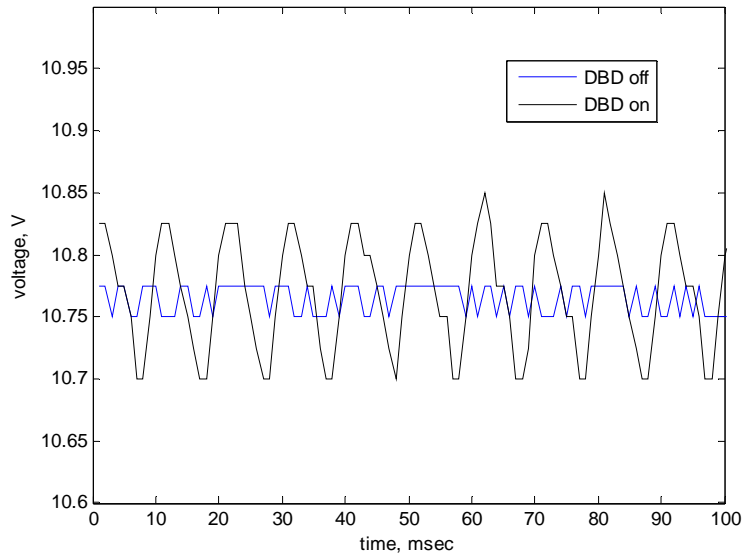


Figure 30 Oscillograms strain-gage signal (Y channel)

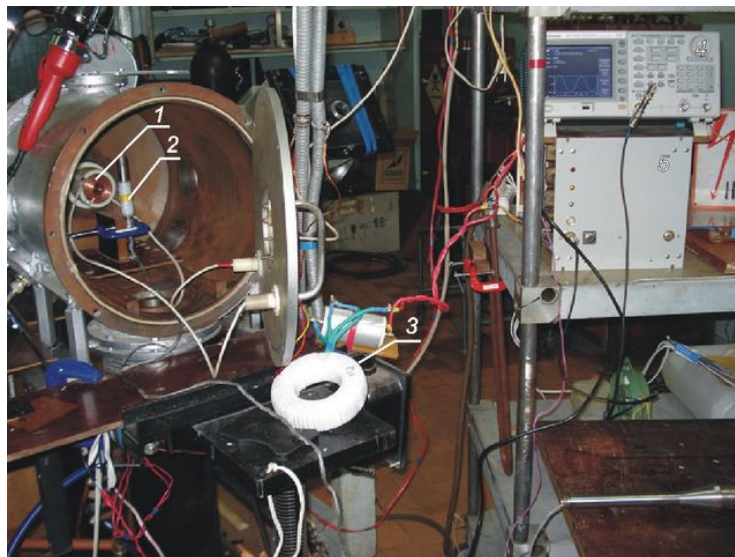


Figure 31 Bench testing of electric systems compatibility (1 – discharge gap, 2 – strain-gage, 3 - transformer)

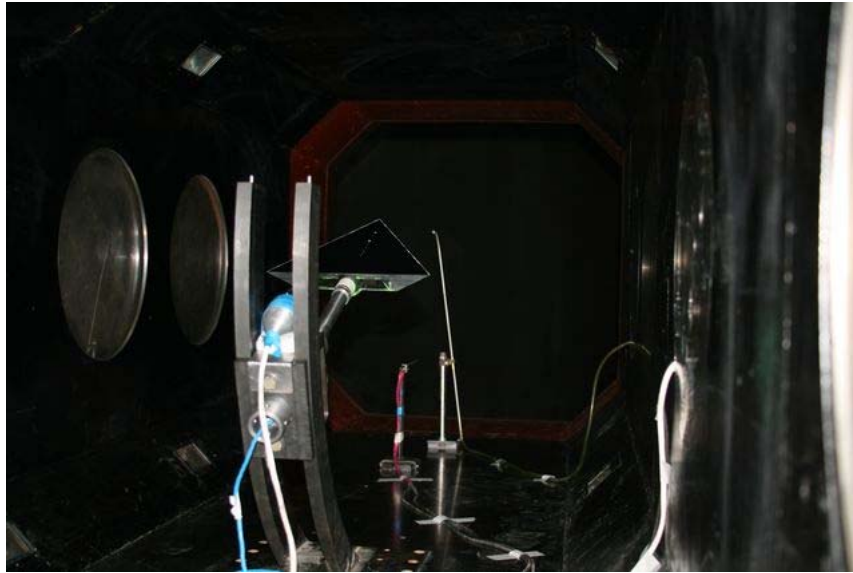
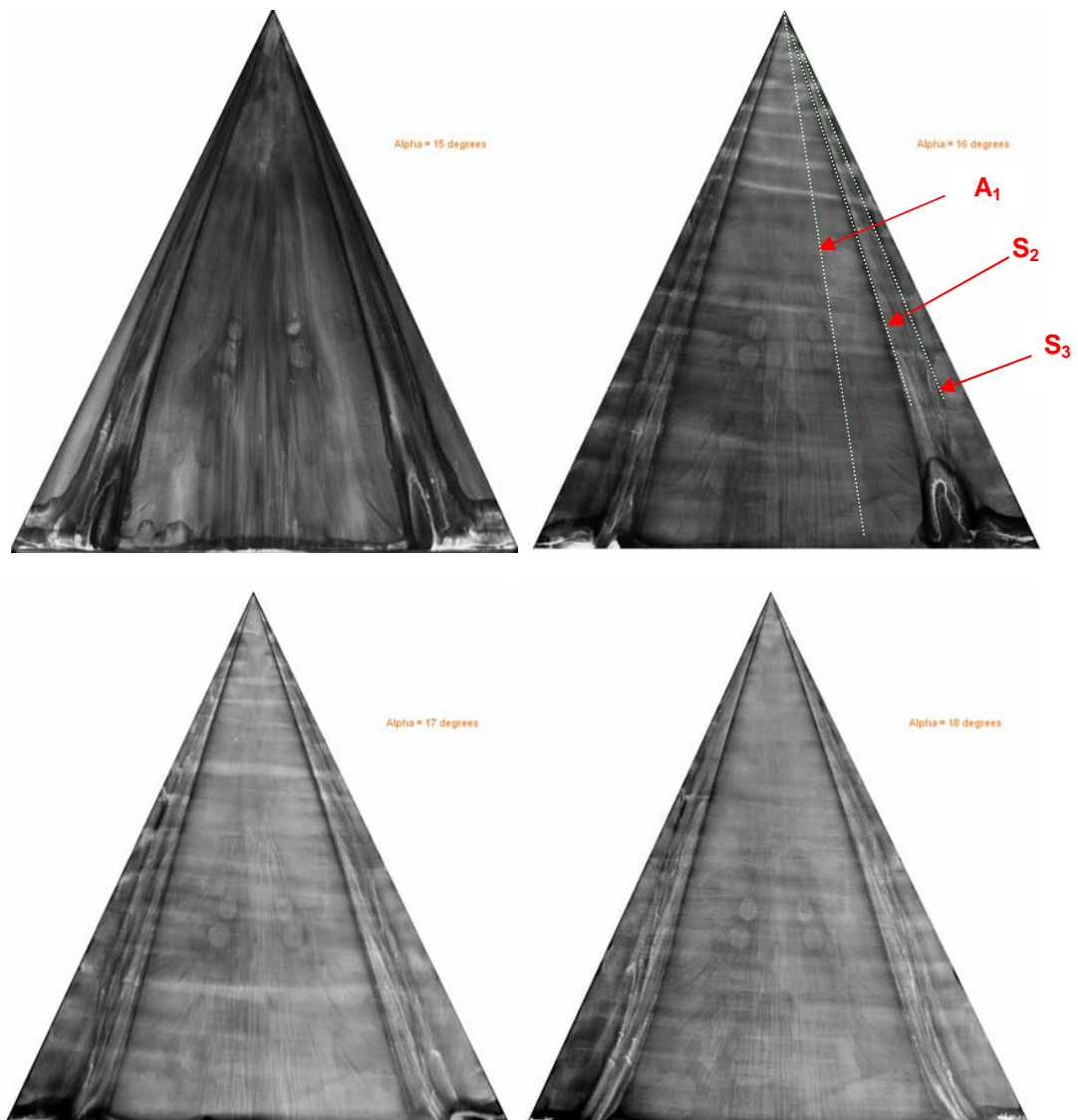
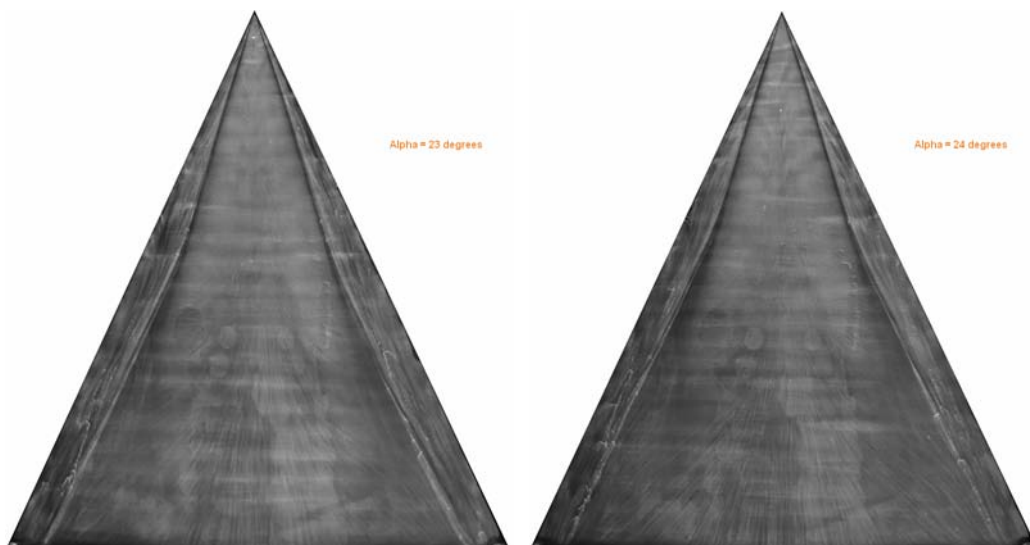
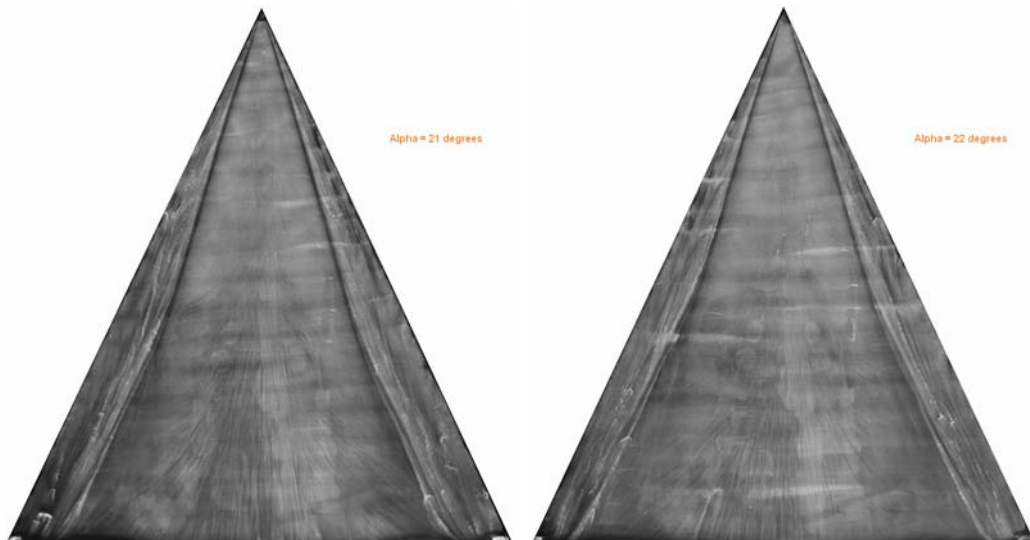
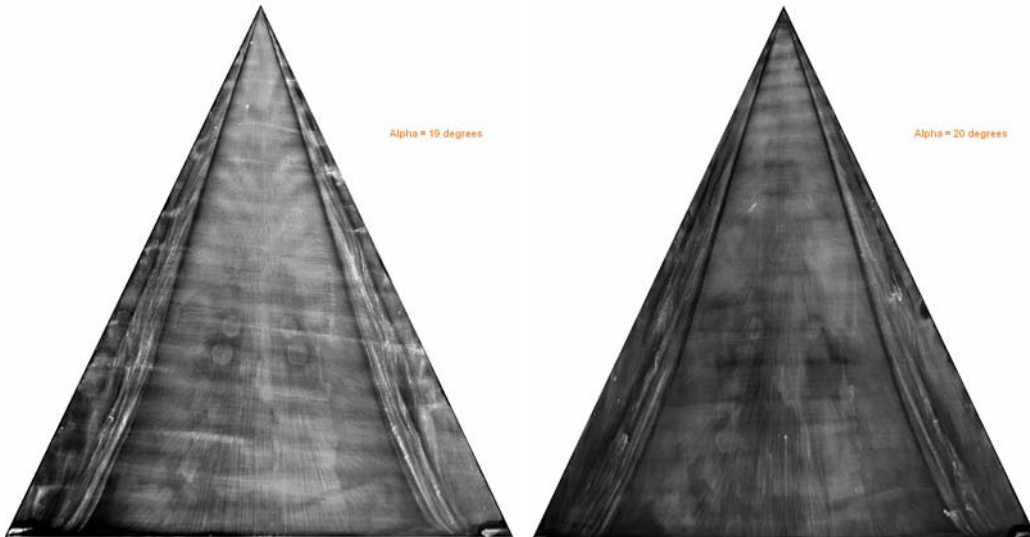


Figure 32 Photo of the model in test section of T-324





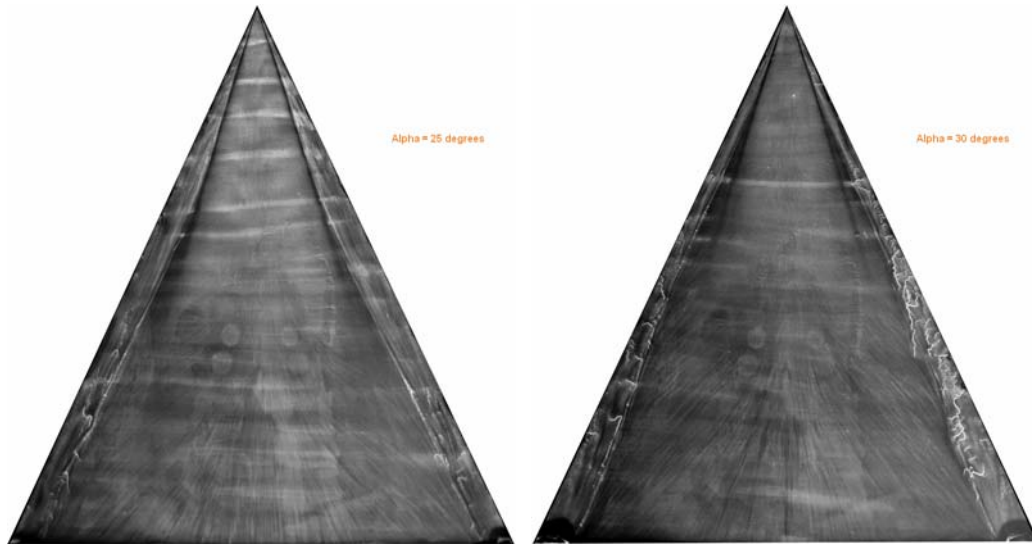


Figure 33 Oil-flow visualization on the leeward side of the delta-wing for various angle of attack ($U_\infty = 12$ m/s)

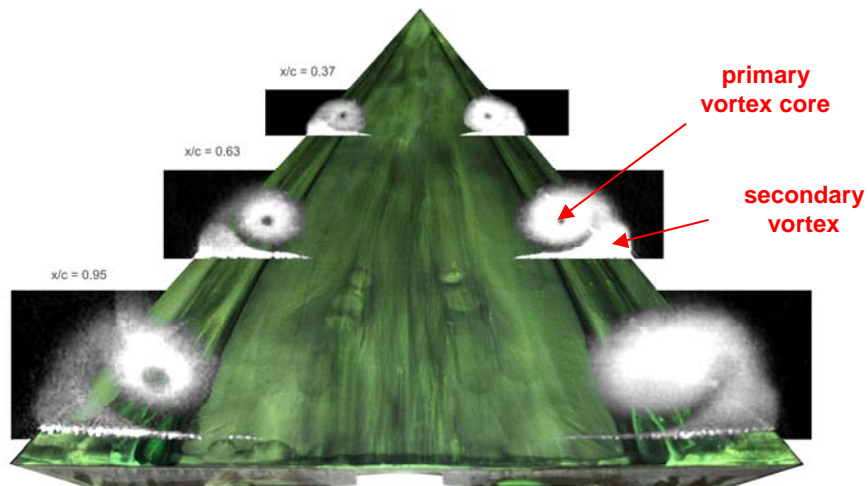


Figure 34 Combined flow visualization ($U_\infty = 12$ m/s, $\alpha = 15^\circ$)

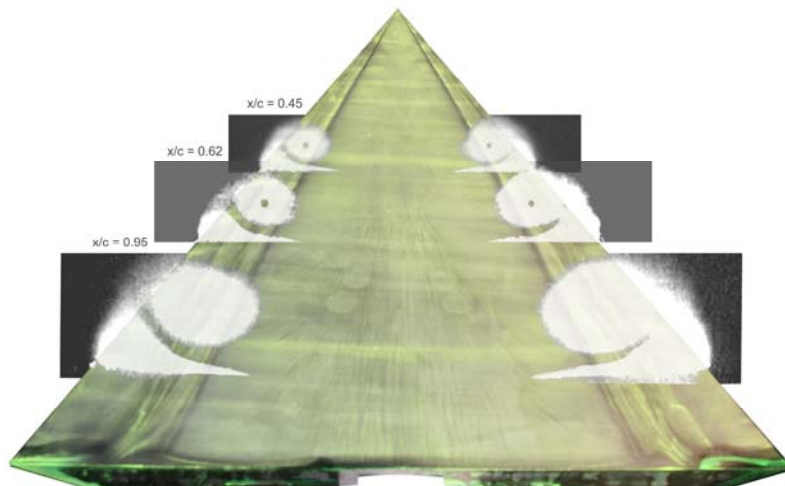


Figure 35 Combined flow visualization ($U_\infty = 12$ m/s, $\alpha = 17^\circ$)

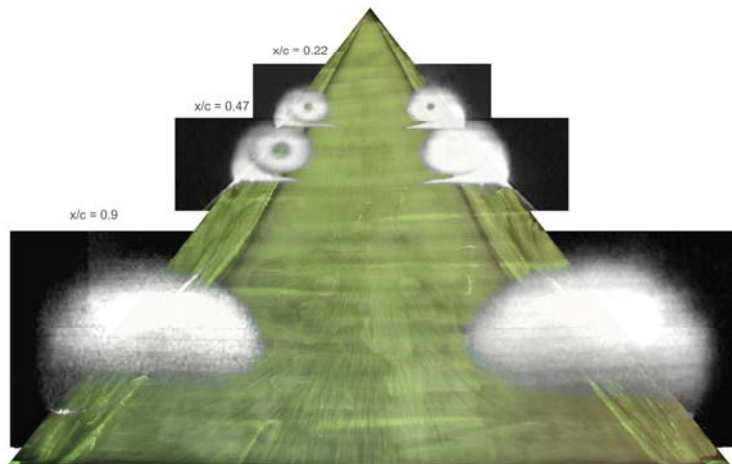


Figure 36 Combined flow visualization ($U_\infty = 12 \text{ m/s}$, $\alpha = 22^\circ$)

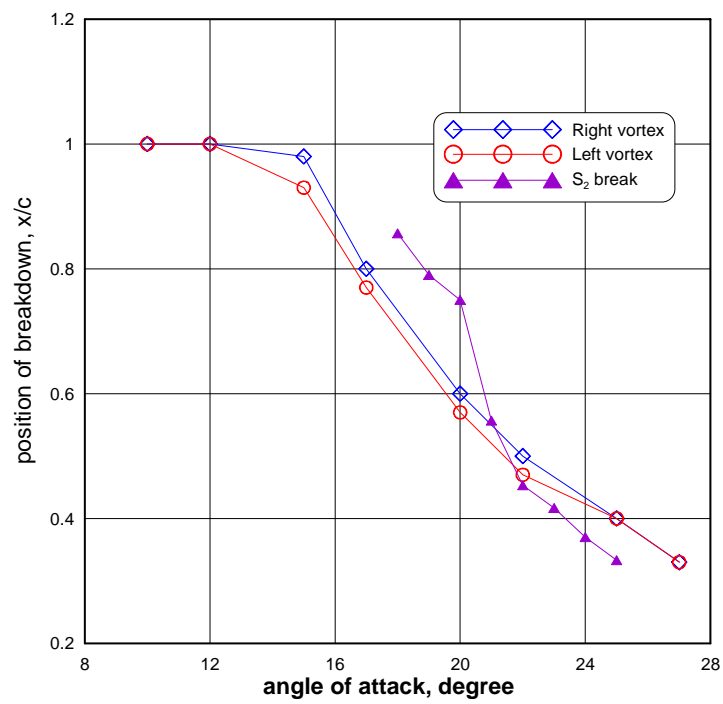


Figure 37 Position of vortex breakdown vs. angle of attack

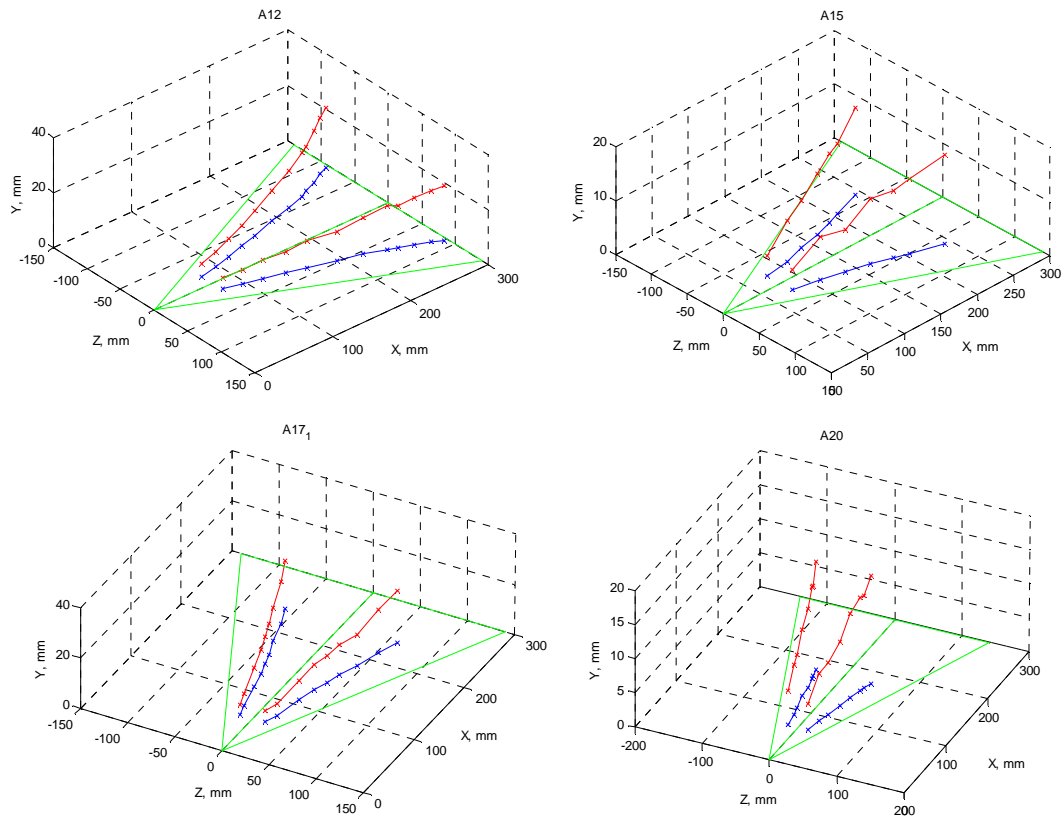


Figure 38 Position of the primary vortexes core

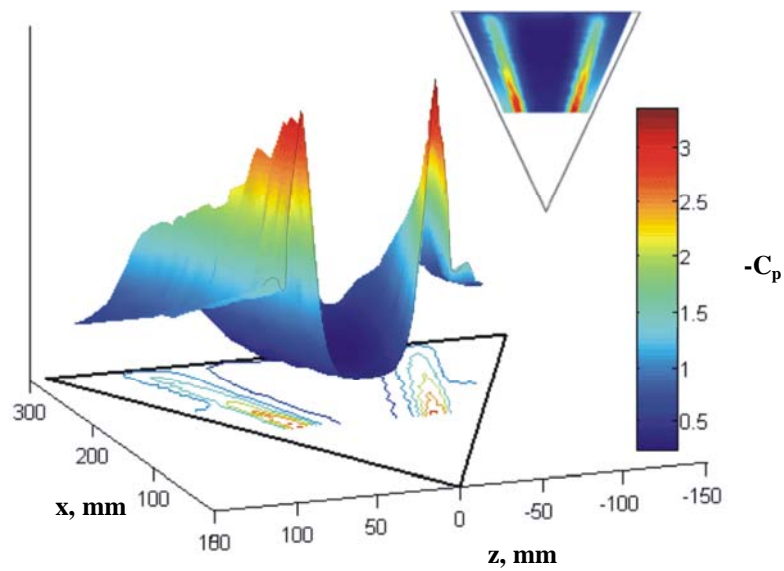


Figure 39 Surface pressure distribution for clean model

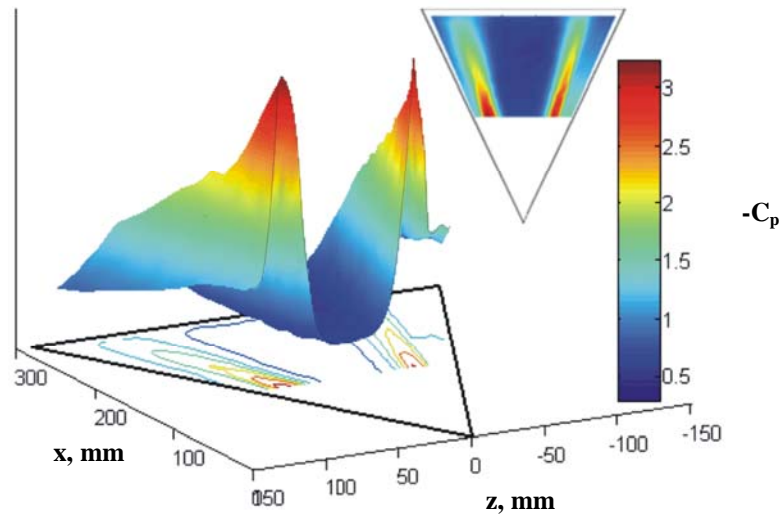


Figure 40 Surface pressure distribution for the model with turbulizer

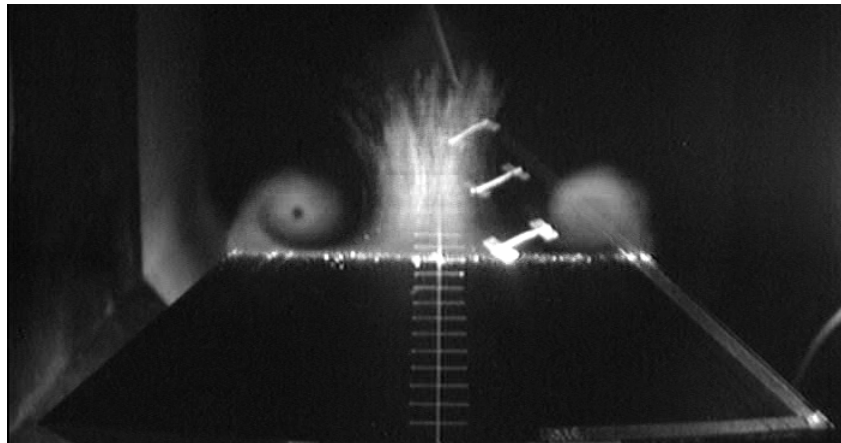


Figure 41 Smoke visualization on the model with turbulizer

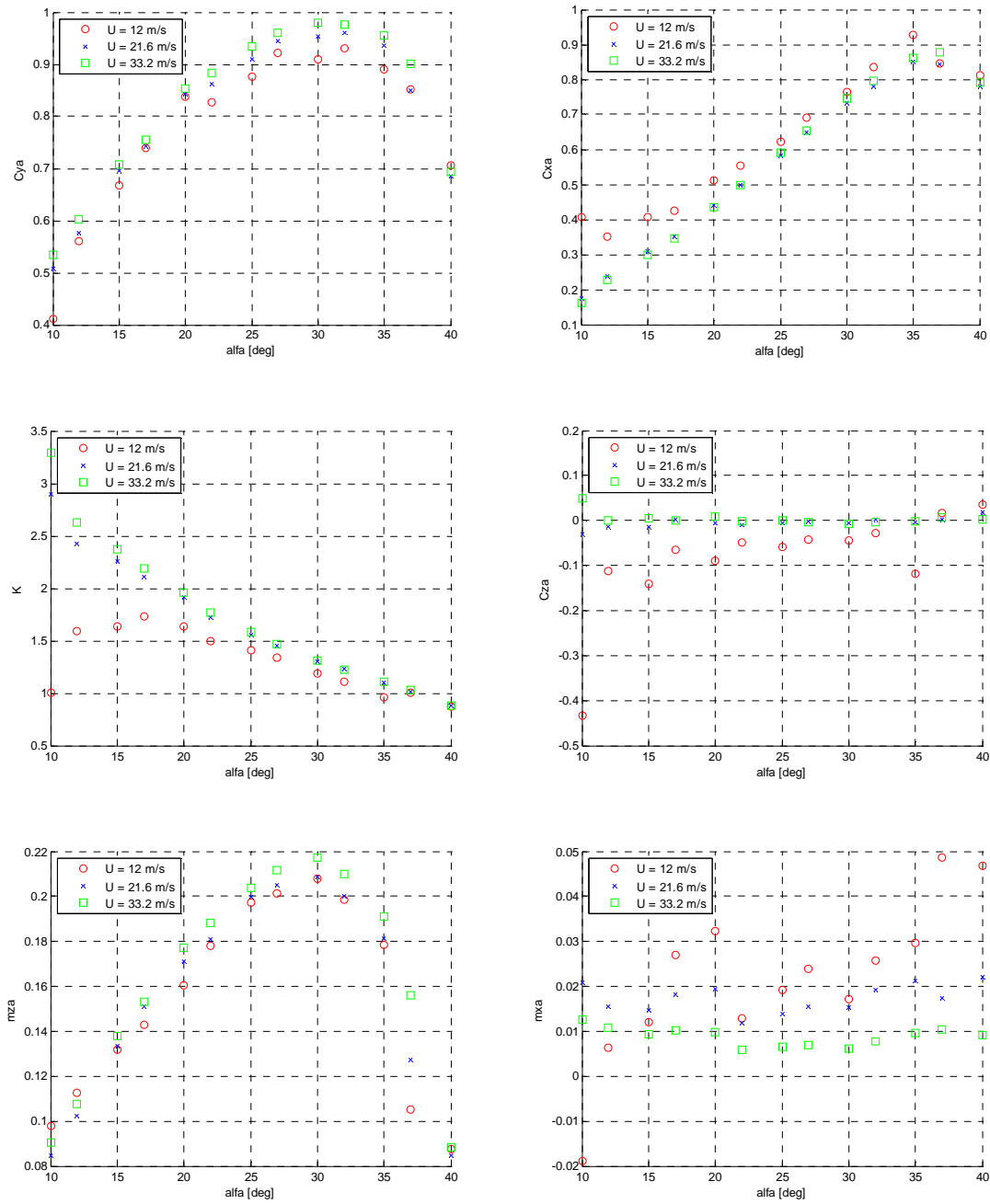


Figure 42 Delta wing characteristics from balance measurements

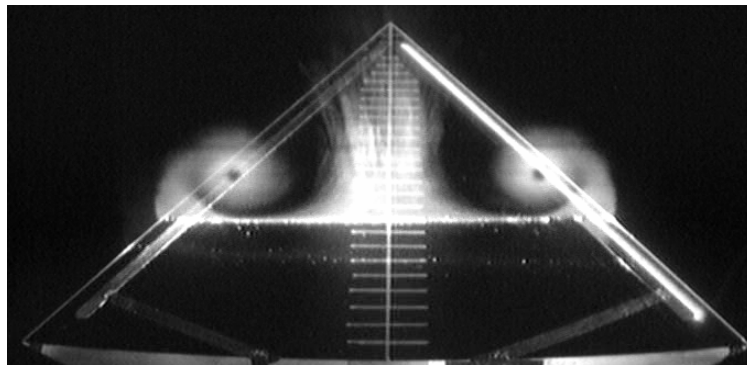


Figure 43 Smoke visualization (actuator on the leading edge, $U_{\infty} = 12 \text{ m/s}$, $\alpha = 17^{\circ}$)

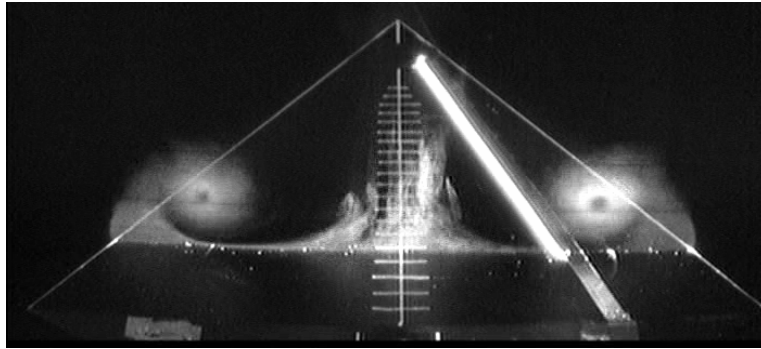


Figure 44 Smoke visualization (actuator on S_2 , $U_\infty = 3$ m/s, $\alpha = 14^\circ$)

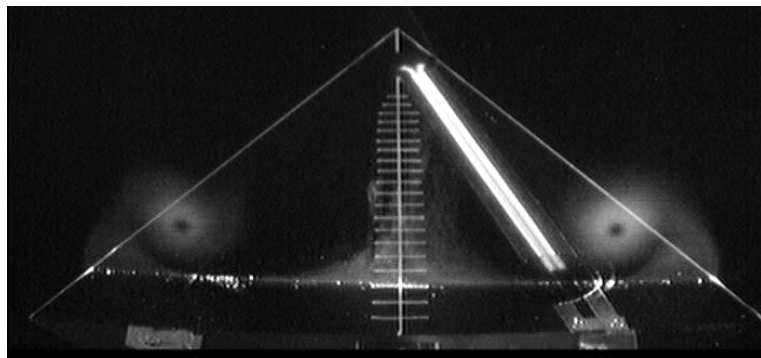


Figure 45 Smoke visualization (PSJ actuator, $U_\infty = 12$ m/s, $\alpha = 14^\circ$)

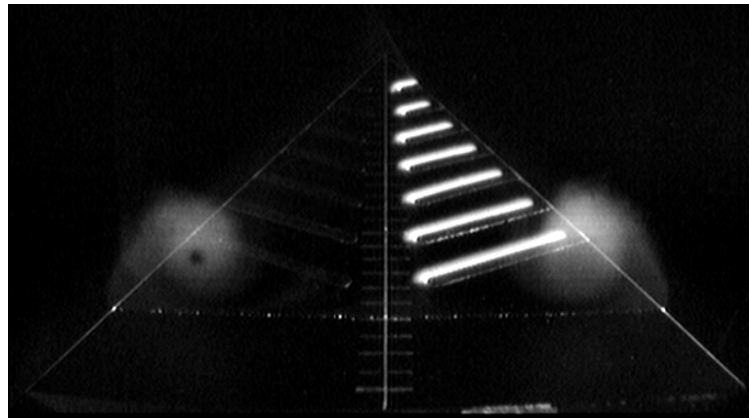


Figure 46 Smoke visualization (actuator across LE, $U_\infty = 12$ m/s, $\alpha = 14^\circ$)